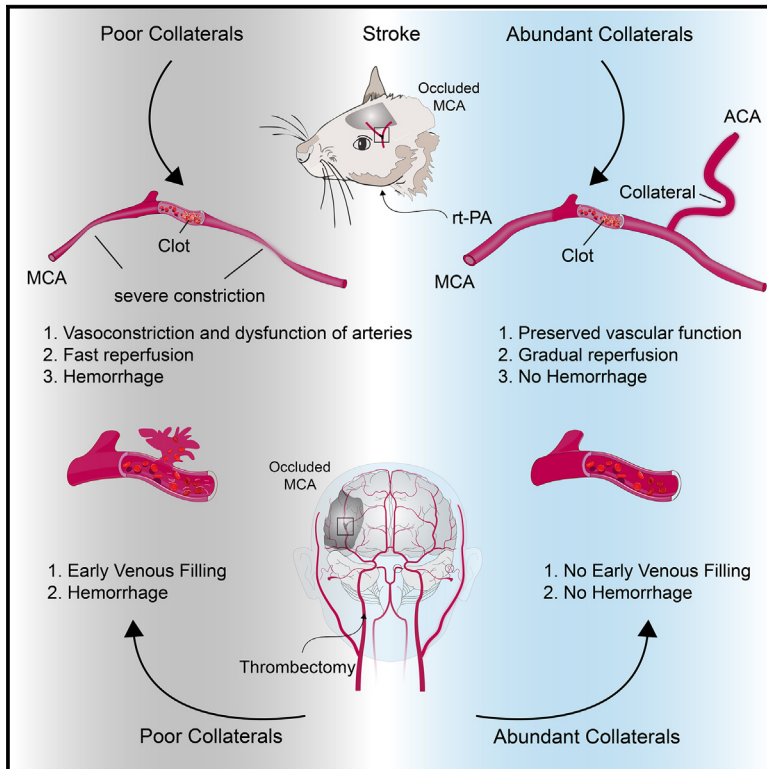# Leptomeningeal collaterals regulate reperfusion in ischemic stroke and rescue the brain from futile recanalization

Graphical abstract

Authors

Nadine Felizitas Binder,
Mohamad El Amki, Chaim Glück, ...,
Michael Weller, Bruno Weber,
Susanne Wegener

Correspondence

susanne.wegener@usz.ch

In brief

Futile recanalization is a serious problem for stroke treatments. Binder and El Amki et al. demonstrate that leptomeningeal collaterals (LMCs) regulate reperfusion after stroke. Mice with poor LMCs developed rapid, uncontrolled hyperperfusion. In stroke patients, they found a similar deleterious reperfusion. Collateral function should be target of novel stroke treatments.

Highlights

- LMCs maintain perfusion during stroke

- Upon recanalization, LMCs allow for a gradual reperfusion

- In mice with poor LMCs, recanalization causes deleterious hyperperfusion

- Stroke patients with poor LMCs show fast reperfusion and futile recanalization

CellPress

Neuron

Article

Leptomeningeal collaterals regulate reperfusion in ischemic stroke and rescue the brain from futile recanalization

Nadine Felizitas Binder,[1,12,13] Mohamad El Amki,[1,12,13] Chaim Glück,[2,12] William Middleham,[1,12] Anna Maria Reuss,[3,12] Adrien Bertolo,[4,5] Patrick Thurner,[6] Thomas Deffieux,[5] Chryso Lambride,[1,11,12] Robert Epp,[10] Hannah-Lea Handelsmann,[1] Philipp Baumgartner,[1] Cyrille Orset,[7] Philipp Bethge,[9,12] Zsolt Kulcsar,[6] Adriano Aguzzi,[3,12] Mickael Tanter,[5] Franca Schmid,[11] Denis Vivien,[7,8] Matthias Tasso Wyss,[2,12] Andreas Luft,[1,12] Michael Weller,[1,12] Bruno Weber,[2,12] and Susanne Wegener[1,12,14,*]

[1]Department of Neurology, University Hospital and University of Zurich, Zürich, Switzerland
[2]Institute of Pharmacology and Toxicology, University of Zurich, Winterthurerstrasse 190, 8057 Zürich, Switzerland
[3]Institute of Neuropathology, University Hospital Zurich, University of Zurich, Schmelzbergstrasse 12, 8091 Zurich, Switzerland
[4]Iconeus, 6 rue Jean Calvin, Paris, France
[5]Physics for Medicine, INSERM U1273, ESPCI Paris, CNRS UMR 8063, PSL Research University, 17 rue Moreau, Paris, France
[6]Department of Neuroradiology, University Hospital and University of Zurich, Zürich, France
[7]Normandie University, UNICAEN, INSERM, Unité Mixte de Recherche-S U1237, Physiopathology and Imaging of Neurological Disorders (PhIND), Institute Blood and Brain @ Caen Normandie, GIP Cyceron, Caen, France
[8]Department of Clinical Research, Caen Normandie University Hospital, Caen, France
[9]Brain Research Institute, University of Zurich, 8057 Zurich, Switzerland
[10]Institute of Fluid Dynamics, ETH Zurich, Zurich, Switzerland
[11]ARTORG Center for Biomedical Engineering Research, University of Bern, Bern, Switzerland
[12]Neuroscience Center Zurich, University of Zurich, ETH Zurich, Zurich, Switzerland
[13]These authors contributed equally
[14]Lead contact
*Correspondence: susanne.wegener@usz.ch
https://doi.org/10.1016/j.neuron.2024.01.031

SUMMARY

Recanalization is the mainstay of ischemic stroke treatment. However, even with timely clot removal, many stroke patients recover poorly. Leptomeningeal collaterals (LMCs) are pial anastomotic vessels with yet-unknown functions. We applied laser speckle imaging, ultrafast ultrasound, and two-photon microscopy in a thrombin-based mouse model of stroke and fibrinolytic treatment to show that LMCs maintain cerebral autoregulation and allow for gradual reperfusion, resulting in small infarcts. In mice with poor LMCs, distal arterial segments collapse, and deleterious hyperemia causes hemorrhage and mortality after recanalization. *In silico* analyses confirm the relevance of LMCs for preserving perfusion in the ischemic region. Accordingly, in stroke patients with poor collaterals undergoing thrombectomy, rapid reperfusion resulted in hemorrhagic transformation and unfavorable recovery. Thus, we identify LMCs as key components regulating reperfusion and preventing futile recanalization after stroke. Future therapeutic interventions should aim to enhance collateral function, allowing for beneficial reperfusion after stroke.

INTRODUCTION

Ischemic stroke, caused by the abrupt blockage of a brain-feeding artery, leads to disability and death in millions of people every year.[1] Current ischemic stroke treatments aim at restoring blood flow by either intravenous thrombolysis, mechanical thrombectomy, or a combination of both.[2] However, despite timely and successful recanalization of the occluded vessel, many patients show insufficient clinical improvement. This has been referred to as "futile recanalization."[3,4] Recanalization is the prerequisite to establish reperfusion, i.e., recovery of blood flow in the brain. Yet, several processes including distal clot fragmentation,[5] pericyte constriction,[6] or neutrophil obstruction of capillaries[7] may hamper reperfusion of the ischemic brain. Therefore, progressive infarct expansion in futile recanalization is caused by reperfusion failure.[8]

Leptomeningeal collaterals (LMCs) are pial anastomotic vessels connecting a fraction of the terminal branches of the middle cerebral artery (MCA) with terminal branches of the anterior

(legend on next page)

Neuron
Article

CellPress
OPEN ACCESS
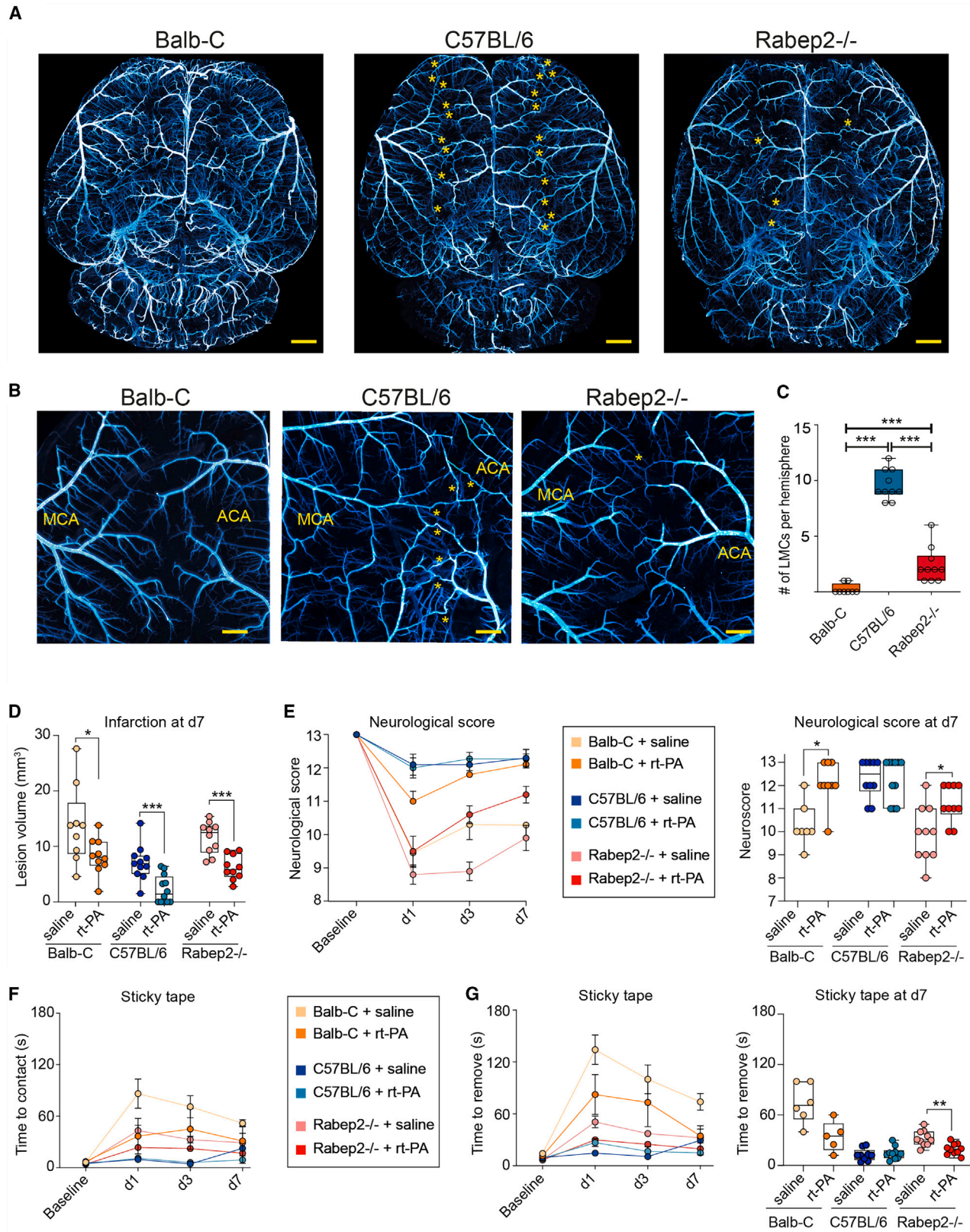
(ACA) and posterior (PCA) cerebral arteries.[9] Although LMCs exhibit minimal flow under normal physiological conditions, when obstruction occurs in a major supply artery, flow across LMCs is recruited and provides partial support of cerebral blood flow (CBF) to the ischemic core and peri-infarct region.[9,10] Recruitment of collateral flow is achieved by vasodilation and a pressure gradient that results in redistribution of flow from neighboring areas to the ischemic tissue.[11,12] The extent of LMCs varies in humans and rodents.[13] In stroke patients, extensive LMCs are associated with better outcome after thrombolysis and mechanical thrombectomy.[14–16] Although LMCs alleviate the severity of ischemic injury, little is known about how differences in collateral extent affect reperfusion after recanalization. In this study, we hypothesized that the presence of abundant LMCs provides hemodynamic support prior to and during reperfusion, thus preventing futile recanalization after stroke therapies.

We used a thrombin model of stroke and thrombolysis in three mouse strains with significant differences in collateral extent. We monitored reperfusion processes *in vivo* to reveal the contributions of LMCs to vessel integrity as well as spatial and temporal dynamics of tissue reperfusion. By *in silico* blood flow modeling, we investigated the spatial impact of collateral extent across vessel types. Finally, we extended these findings from mice to patients with acute ischemic stroke that received thrombectomy providing direct translational evidence in support of a protective role of LMCs during reperfusion.

RESULTS

Variation of LMC amount in selected mouse strains

To contrast arterial networks with different extents of LMCs, we examined C57BL/6, Rabep2−/−, and Balb-C mice.[17,18] Rabep2−/− mice have a C57BL/6 background but, due to a disruption of the Rabep2 gene previously shown to be important in LMC formation during development, have a reduced number of LMCs.[17,19,20] For 3D vessel visualization and LMC quantification, we performed brain clearing and immunostaining based on iDISCO.[21] We imaged smooth muscle actin (α-SMA)-positive cells throughout the entire brain using light sheet microscopy (Figures 1A, 1B, and S1).[22] LMCs were defined as α-SMA-positive vessels anastomosing opposing distal branches of the MCA and ACA. Consistent with previous reports,[16,21] we observed an average of approximately 10 MCA-ACA collaterals per hemisphere in C57BL/6 and 2–3 in Rabep2−/− mice, and none in most (occasionally 1) Balb-C mice (Figure 1C). Thus, we denoted LMCs as "abundant" in C57BL/6, "intermediate-to-poor" in abundance in Rabep2−/−, and "poor" in Balb-C animals.

Thrombolysis-induced MCA recanalization is independent of LMC extent

Next, we sought to determine whether the presence of LMCs impact clot formation and the dissolution processes during thrombolysis. We employed the thrombin model of stroke in C57BL/6, Rabep2−/−, and Balb-C mice (Figures S2 and S3).[23,24] This model closely mimics the clinical situation of stroke patients with natural clot formation and rt-PA-based intravenous thrombolysis, allowing for direct *in vivo* visualization of reperfusion. We investigated the formation of the clot after thrombin microinjection and clot presence at 2 h post-stroke (90 min after the start of rt-PA or vehicle infusion). Independent of strain, thrombin injection led to an occlusion of the MCA at its M2 bifurcation, which persisted for 2 h in 60%–75% of the control-treated mice. Rt-PA infusion at 30 min after stroke induction led to complete or partial MCA-M2 recanalization (Balb-C: 94.1%; C57BL/6: 95.3%; Rabep2−/−: 92.9%) independent of LMC status (Figure S2). In all strains, ischemia durations were kept constant. Thus, we did not observe that more abundant LMCs augmented clot dissolution on thrombolytic treatments and enhanced recanalization.

Stroke outcome is associated with number of LMCs

We then tested whether abundant LMCs preserve tissue integrity and neurological function in stroke. Mice receiving either rt-PA or vehicle were monitored for 7 days after induction of stroke. Infarct volumes on day 7 were largest in Balb-C, intermediate in Rabep2−/−, and smallest in C57BL/6 mice (Figures 1D–1G), confirming previous studies employing permanent distal M1-MCA ligation wherein robust collateral circulation limited infarct size.[19] Thrombolysis significantly reduced ischemic tissue damage in all three strains compared with control treatment (Balb-C: 13.84 ± 2.34 mm^3 vs. 8.22 ± 1.01 mm^3; Rabep2−/−: 11.59 ± 0.91 mm^3 vs. 6.24 ± 0.70 mm^3; C57BL/6: 7.07 ± 0.96 mm^3 vs. 2.26 ± 0.72 mm^3) (Figure 1D). This was reflected in better sensorimotor function after rt-PA in Balb-C and Rabep2−/−, but not in C57BL/6 mice, which showed only minimal deficits overall (Figure 1E). In general, sensorimotor functions assessed by the sticky tape test and a composite neurological score were better for C57BL/6 mice, which, having abundant LMCs, experienced only minimal deficits (Figures 1E–1G and S4).

LMCs are recruited during stroke and reperfusion

To examine the contribution of LMCs to stroke and reperfusion, we performed *in vivo* two-photon imaging in the MCA-ACA watershed area of C57BL/6 mice (Figure 2). Immediately after stroke, LMCs underwent dilation, and collateral flow was recruited from the ACA to the MCA territory (Figures 2D and 2E). Following recanalization of the MCA, collateral diameter and

Figure 1. Quantification of LMCs, infarct volume, and sensorimotor function in Balb-C, C57BL/6, and Rabep2–/– mice
(A) Representative overview images of iDISCO cleared and anti-SMA-Cy3 stained brains of Balb-C, C57BL/6, and Rabep2−/− mice. Yellow stars indicate LMCs. Scale bar, 1 mm.
(B) Close-up images of watershed area, yellow stars indicate LMCs. Scale bar, 200 μm.
(C) Quantification of LMCs per hemisphere in all three strains (n = 5 per strain). Note that LMC numbers of Balb-C and C57BL6 are similar to Chalothorn et al.,[18] who used fluorescent angiography. We here show that numbers are intermediate-to-poor in Rabep2−/− mice, ***p < 0.001; in two-tailed Mann-Whitney U test.
(D) Bar graph depicting infarct volumes from individual mice from the three different strains at day 7, *p < 0.05, ***p < 0.001 in two-tailed Mann-Whitney U test.
(E–G) Neurological score and sticky tape removal assessment in saline and rt-PA-treated mice at days 1, 3, and 7 after stroke. *p < 0.05, **p < 0.01 in two-tailed Mann-Whitney U test, n = 10.
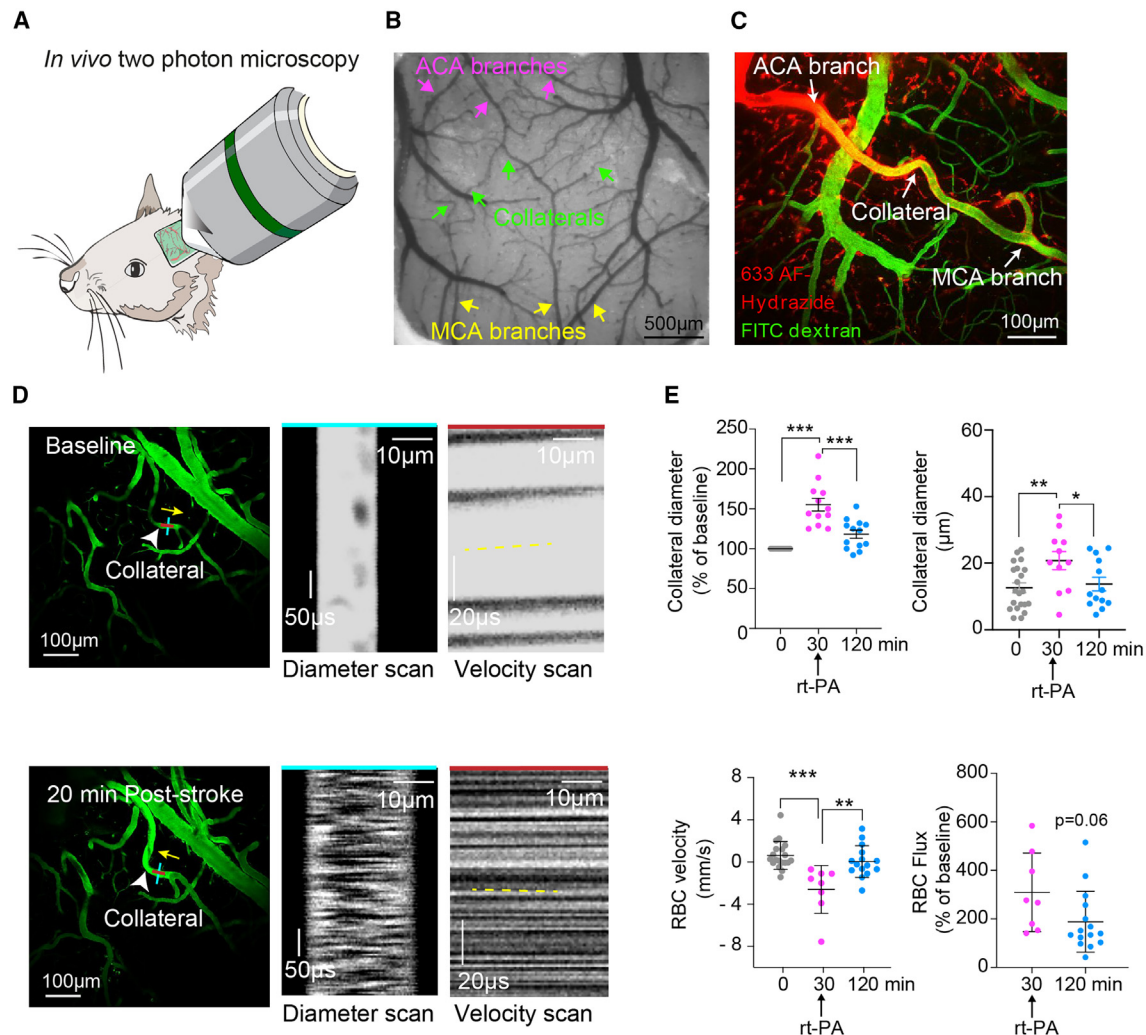
Figure 2. Two-photon imaging of LMCs pre- and post-stroke in C57BL/6 mice
(A) Schematic drawing of two-photon setup.
(B) Cranial window of C57BL/6 mouse. This strain was used here because it has extensive LMCs. Arrowheads displaying MCA branches and LMCs.
(C) Image during two-photon acquisition. Blood plasma is labeled in green using fluorescein isothiocyanate (FITC) dextran. To differentiate arteries from veins, 633 Alexa Fluor (AF)- hydrazide (red) staining was used (arterial vessel wall in red).
(D) On the left, representative image of LMC response to stroke in C57BL/6 mice. In the middle, kymographs of LMC diameter changes post-stroke, generated by transverse line scans (blue lines in left images). On the right, kymographs of red blood cell flow in collaterals in baseline and post-stroke generated by line scans parallel to the flow (red lines in left images). Dark streaks represent red blood cells, gray streaks represent the fluorescent tracer-filled LMC lumen.
(E) LMC diameter, RBC velocity, and flux changes in C57BL/6 at baseline (0), 30, and 120 min after stroke induction; **p < 0.01; ***p < 0.001 two-tailed t test, n = 5.

flow returned to baseline values, demonstrating the contribution of LMCs to blood flow toward the occluded territory. In LMCs of Rabep2−/− mice (due to the low amount of LMCs present, only very few could be visualized under the cranial window), two-photon imaging confirmed a similar stroke-induced dilation and flow increase, normalizing after recanalization (Figure S5). Therefore, LMCs are indeed recruited during stroke, augmenting flow toward the affected territory.

The extent of LMCs affects the level of flow recruitment
To comment on flow recruitment across descending arterioles (DAs) and capillaries (Cs) and in function of the number of LMCs,

we used blood flow simulations in four semi-realistic microvascular networks derived from realistic surface arteriole (SA) networks from 2 C57BL/6 and 2 Balb-C mice.[12] The SA networks were extended by penetrating trees (DAs and ascending venules, AVs) and an artificially generated capillary bed (Figure 3A), and the number of LMCs was manually modified to generate representations with high (100% LMC), intermediate (50% LMC), and no collaterals (0% LMC) (Figure 3B). Consequently, the networks only differed in the number of LMCs, which allowed us to estimate the impact of the extent of LMCs in an isolated manner.

The integral flow rate through the DA root points at the cortical surface, which is a direct measure of the flow reaching the

CellPress
OPEN ACCESS

(legend on next page)

CellPress
OPEN ACCESS
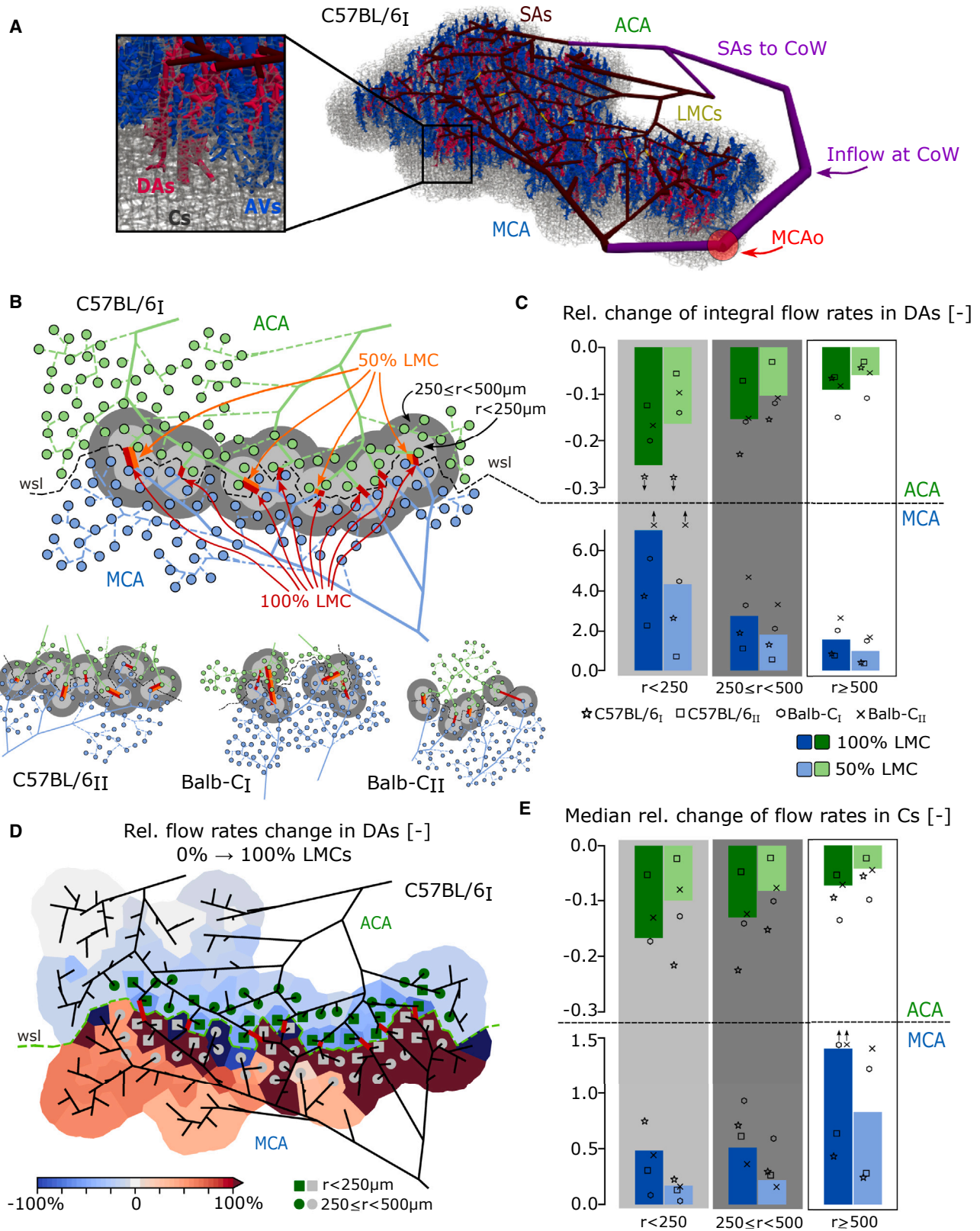
Neuron
Article

capillary bed, clearly showed that blood flow is redistributed from the ACA to the MCA side and that this effect was most pronounced for 100% LMCs and in proximity to the LMCs (Figures 3C and 3D). On the MCA side, the integral perfusion of DA roots was 714% larger for 100% LMC compared with 0% LMC (<250 μm) and remained 154% larger 500 μm distal from the LMCs. The median relative change in capillary flow rate is another metric to assess how flow is distributed to individual capillaries in an averaged manner (Figure 3E). In line with the integral DA root flow, we consistently observed that the median capillary flow rate change was larger for 100% LMC (e.g., 48% vs. 17% increase for 100% LMC and 50% LMC, respectively, at <250 μm).

LMCs affect the dynamics of blood flow recovery during reperfusion

Having documented recruitment of LMCs during ischemia and reperfusion at the single-vessel level, we next explored the effects of LMC recruitment on recovery of blood flow to the ischemic territory during thrombolysis. Laser speckle contrast imaging (LSCI) was used to provide continuous wide-field perfusion assessment with high temporal resolution and spatial resolution at a depth of 300–700 μm[25] at baseline, during, and for 120 min after thrombin occlusion (Figures 4A and 4B). After occlusion of the MCA, all three strains evidenced a significant drop in perfusion of the distal MCA territory (M4/M5 territory) to 20%–30% of baseline (Figures 4B–4D). Cortical perfusion remained low for 120 min after induction of stroke followed by sham-thrombolysis (Figures 4B, 4C, and S6). Significant reperfusion followed rt-PA administration in Balb-C and Rabep2−/− mice (60.2% ± 3.77% and 59.2% ± 3.66% of baseline). Surprisingly, in C57BL/6 mice with abundant collaterals and irrespective of rt-PA administration, CBF recovered more slowly and to only about 50% of baseline (47.3% ± 4.27% vs. 47.7% ± 4.53%) (Figures 4B and 4D).

Based on the above discrepancy between slower and less cortical reperfusion in the MCA-M4/M5 territory, yet excellent functional and tissue outcome in C57BL/6 mice (abundant collaterals), we hypothesized that LMCs facilitate reperfusion of more proximal territory in C57BL/6 mice that is not accessible to LSCI. Therefore, we next used ultrafast ultrasound (uUS) with 4D ultrasensitive Doppler recordings and ultrasound localization microscopy (ULM)[26] to investigate the more proximal MCA-supplied areas, just distal to the site of thrombin microinjection and clot formation.

We next applied uUS to measure cerebral blood volume (CBV) in deep (8 mm maximum) tissue during stroke and thrombolysis

for 2 h (Figure 5). Although remote areas as the striatum showed no differences between the strains (Figure S7), we evaluated CBV in the MCA-M4/M5 territory that had been assessed with LSCI in the previous experiment shown in Figure 4. Consistent with the LSCI findings, thrombolysis resulted in higher reperfusion levels within the area supplied by the MCA-M4/M5 in mice with poor and poor-to-intermediate LMCs (Balb-C, Rabep2−/−), compared with animals with abundant LMCs (C57BL/6) (Figure S8). In agreement with our previous LSCI results, complete reperfusion was not achieved in this superficial cortical region. However, in more proximal MCA-M3 territory, thrombolysis resulted in reperfusion to, or exceeding 100% of baseline in all three strains (Figure 5C), indicating that recanalization-induced reperfusion of proximal and distal MCA-supplied brain areas varied greatly depending on LMC status: mice with poor or poor-to-intermediate LMCs showed hyperaemic (above 100% baseline) reperfusion in the affected M3 territory (Balb-C 138.8% ± 23.1%, Rabep2−/− 145.8% ± 20.3%) (Figure 5C). This hyperaemic reperfusion upstream (MCA-M3) in poor and intermediate-poor collateral mice was likely the cause for the higher perfusion levels reached at the downstream MCA-M4/M5 segment. Furthermore, the time to reach pre-stroke baseline perfusion levels after thrombolysis was also notably different: mice with abundant LMCs underwent gradual reperfusion, reaching 100% of pre-stroke values in 98.5 ±7.77 min. By contrast, mice with poor or poor-to-intermediate LMCs underwent significantly earlier (Balb-C) and faster/steeper rates of reperfusion (Balb-C and Rabep2−/−), reaching 100% at 66.37 ± 12.59 (Balb-C) or 83.7 ± 9.54 min (Rabep2−/−), respectively.

Rapid reperfusion and hyperemia in mice with poor collaterals are associated with loss of vascular tone in distal MCA branch segments

To reveal the structural and hemodynamic underpinnings of the observed different reperfusion responses, we used intravital two-photon microscopy (Figure 6). We analyzed diameter and blood flow in the distal MCA branches (MCA-M5 segment) in Balb-C, C57BL/6, and Rabep2−/− mice during stroke and reperfusion. Following MCA occlusion, all animals sustained a large decrease in red blood cell (RBC) velocity in the MCA-M5 segment (Figure 6C). The drop in blood flow was less severe in C57BL/6 mice (abundant collaterals), suggesting that abundant LMCs maintain residual perfusion to the outer MCA territory after occlusion. Interestingly, the diameter of M5 segment arterioles as assessed between 15 and 30 min after thrombin occlusion declined significantly in Balb-C mice with poor collaterals, while

---

Figure 3. Changes in blood flow rate in response to middle cerebral artery occlusion (MCAo) and arterial dilation for different extents of LMCs

(A) Semi-realistic microvascular network (MVN) based on the realistic surface arteriole (SA) network of a C57BL/6 mouse. The zoom-in depicts the added penetrating trees (descending arterioles, DAs, and ascending venules, AVs) and the artificial capillary bed (Cs). At the surface, MCA and ACA feeding vessels are connected to the circle of Willis (SAs to CoW), and the location of MCAo is included.

(B) The four SA networks derived from 2 C57BL/6 and 2 Balb-C mice. Green and blue depict SAs in the ACA and MCA territories, respectively. LMCs for the 50% and 100% LMC configurations are highlighted in orange and red, respectively. The gray shaded areas mark the regions that are closer than 250 μm (light gray) or between 250 and 500 μm (dark gray) to an LMC start/endpoint. wsl: watershed line.

(C) Relative change in integral blood flow through MCA- and ACA-sided DA root points for the 100% LMC and the 50% LMC configurations with respect to 0% LMC. The bars depict the mean across the four semi-realistic MVNs. Relative changes are displayed for three distance categories to LMC start/endpoints < 250 μm, 250–500 μm, and ≥ 500 μm (see B).

(D) Relative change in blood flow between 100% LMC and 0% LMC for individual DA root points for C57BL/6_I.

(E) Median relative change of capillary blood flow rates displayed equivalently to (C).
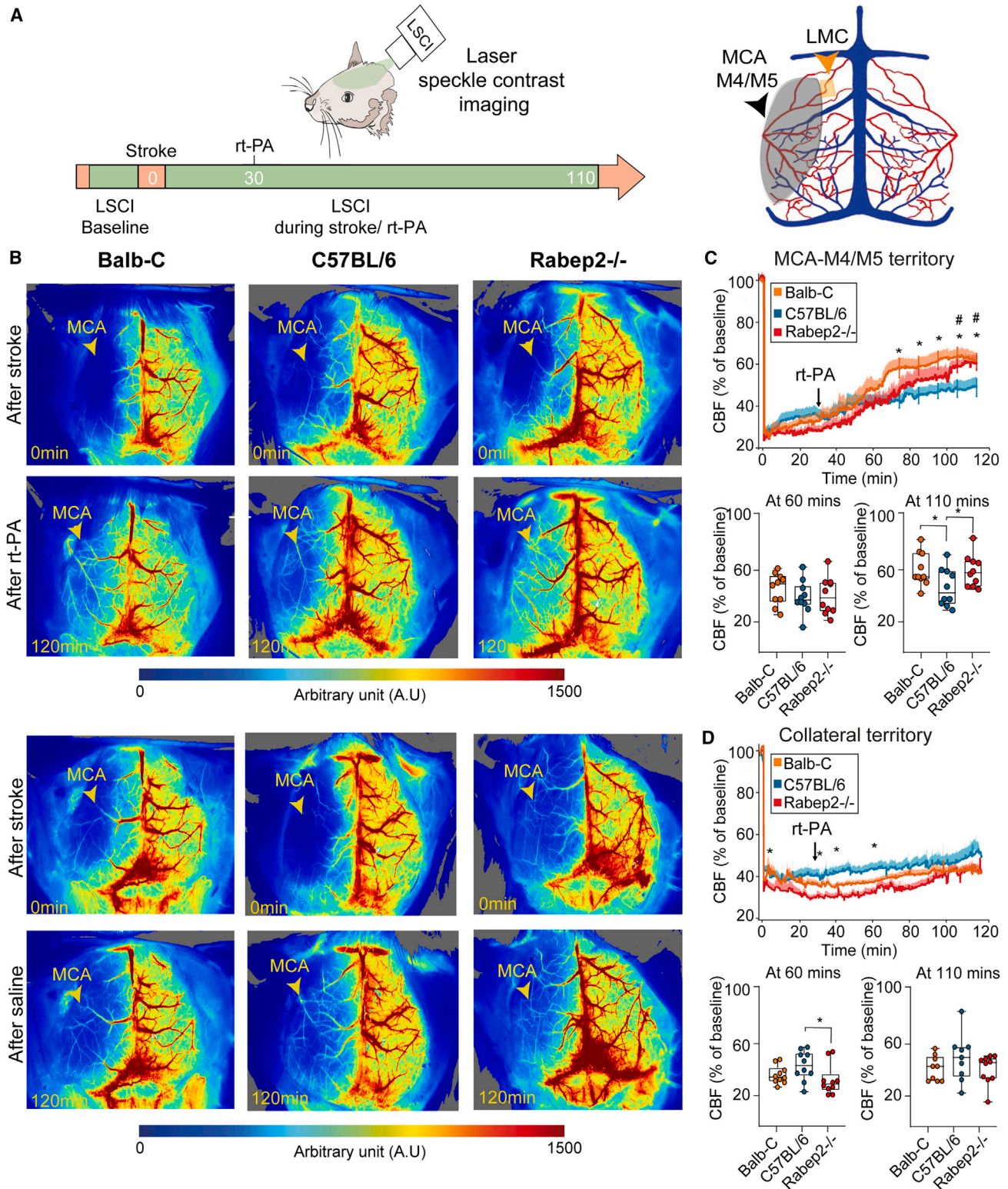
Figure 4. Reperfusion after thrombin occlusion and thrombolysis assessed by LSCI

(A) Experimental setup, containing 110 min post-stroke CBF monitoring (left). Schematic drawing of the LSCI view on pial vessels and the MCA-M4/M5 region as well as the watershed territory used for analyses (right).

CellPress
OPEN ACCESS

Neuron
Article

reduction in diameter was much less in Rabep2−/− and absent in C57BL/6 mice (Figures 6B, 6C, and S9).

To test whether the decline in diameter reflected a loss of vessel function, we assessed cerebrovascular reactivity. During pre-stroke and post-thrombolysis conditions, mice received a 5 min CO_2 challenge via facemask, while we measured perfusion using LSCI (Figures 6D and S10). During baseline, hypercapnia induced an increase in CBF to 137.3% ± 10.64% (Balb-C), 144.1% ± 7.31% (C57BL/6), and 140% ± 5.45% (Rabep2−/−) within the MCA-M5 supplied territory (Figure 6E). However, when challenged 60 min after thrombin microinjection and 30 min after start of rt-PA infusion, the hyperemic response was attenuated in Balb-C to 113.4% ± 8.94% and Rabep2−/− to 111.3% ± 3.02%, while preserved in C57BL/6 mice (141.5% ± 8.44%) (Figures 6F and S10). These data indicate a loss of vascular regulation capacity in distal blood vessels after clot removal in mice with poor and poor-intermediate LMCs.

Rapid hyperemia in mice with poor collaterals associates with intracerebral hemorrhage and poor functional outcome

Given that intracerebral hemorrhage (ICH) is a major complication of recanalization treatments after stroke, we asked whether the hyperemic reperfusion in mice with poor LMCs was associated with tissue injury. Therefore, we analyzed mortality and occurrence of ICH for up to 7 days after stroke. 40% of all rt-PA treated Balb-C mice died in the subacute phase after stroke (days 1 to 4), while no mortality occurred in Rabep2−/− nor C57BL/6 mice (Figures 7A and 7B). LSCI analysis of the MCA-M4/M5 territory revealed that animals that died prematurely displayed significantly faster reperfusion that reached higher values in the initial 2 h after stroke, compared with the ones surviving (Figure 7C). Notably, even within the group of Balb-C animals (poor LMCs) with rt-PA thrombolysis, significantly higher reperfusion levels were reached in animals that died vs. those that survived (Figure S11A). Furthermore, all rt-PA treated Balb-C and a subset of Rabep2−/− treated animals showed evidence of ICHs after reperfusion, while none of the C57BL/6 mice did (Figure 7D). CBF curves of animals with ICH were characterized a faster (steeper) reperfusion compared with animals without ICHs in the first 2 h after stroke (Figures 7F and S11B). These data demonstrate that a fast and steep reperfusion in cortical areas supplied by the MCA-M4/M5 segment was associated with a higher risk of complications (ICH/death).

Early venous filling in stroke patients undergoing thrombectomy indicates unfavorable outcome

Finally, we explored whether the observed reperfusion patterns in mice with different extents of LMCs and their association with stroke treatment outcome could be of relevance for stroke patients. The only direct assessment of reperfusion after stroke treatment is the immediate post-interventional DSA from pa-

tients with large vessel occlusion (LVO) stroke undergoing thrombectomy. We examined whether rapid reperfusion after recanalization of a large vessel occurred in stroke patients associated with poor collateral status and adverse outcomes. Out of 96 patients undergoing intra-arterial treatment for ischemic stroke at the University Hospital Zurich Stroke Center between 01-07/2021, we included data of 33 patients with distal MCA-M1 or M2 occlusion who had successful recanalization (modified treatment in cerebral infarction, mTICI[27] grade 2b or 3). We excluded patients with additional ipsilateral carotid artery stenosis or occlusion, distal clot embolism, without clinical follow-up according to the modified Rankin Scale (mRS) at 3 months, and patients who declined use of their data for research (see patient flow chart on Figure S12). Post-thrombectomy data from DSA were color-coded according to the time of contrast filling (in seconds; Figure 8). From these time-coded DSA series, two senior neuroradiologists blinded to patient outcome or follow-up imaging categorized patients into those with early venous filling (n = 23) and without early venous filling (n = 10) after thrombectomy, approximating the rapid vs. slow reperfusion pattern observed in the rodent stroke model. The two groups were then compared regarding clinical characteristics (age and sex), collateral score (poor, moderate, and good based on pre-thrombectomy CT angiography data), initial stroke severity (National Institutes of Health Score, National Institute of Health Stroke Scale [NIHSS] on admission), hemorrhagic transformation on follow-up imaging after 1 day, and clinical outcome (mRS and NIHSS after 3 months) (Figure 8E). Patients with early venous filling had significantly lower collateral scores (p = 0.002) and more remaining neurological deficits at 3 months (NIHSS 1 [IQR4] vs. 0 [IQR 0], p = 0.041) compared with those without early venous filling. Furthermore, hemorrhagic transformation of the infarcted area was detected only in patients with early venous filling (47.8% vs. 0%; p = 0.007), suggesting a reduction in structural integrity of the vasculature in the infarcted areas. Both collateral score and early venous filling were correlated with NIHSS at 3 months (Spearman's Rho (ρ (rho)) = −5.08, p = 0.009 and ρ (rho) = 0.417, p = 0.038), while only collateral score was correlated with mRS at 3 months (ρ (rho)) = −3.56, p = 0.042 and ρ (rho) = 0.272, p = 0.125). Early venous filling showed a strong correlation with hemorrhagic transformation (ρ (rho) = 0.466, p = 0.006).

DISCUSSION

Futile recanalization, i.e., insufficient clinical and tissue recovery despite successful clot removal in stroke, is an immense clinical problem. Its underlying mechanisms remain poorly understood. Insufficient reperfusion of the microvascular bed or accelerated tissue injury upon reperfusion have been previously discussed.[28–30] Extensive collaterals have been associated with better outcome in stroke and recanalization

---

(B) Representative LSCI images showing cortical perfusion after stroke induction (upper row) and treatment (bottom row) in rt-PA (upper two panels) and sham treated (lower two panels) Balb-C, C57BL/6, and Rabep2−/− mice at 2 h after stroke. Arrowhead indicating perfusion status of MCA branch.

(C and D) LSCI recordings for the (C) MCA-M4/M5 and (D) watershed territory compared with baseline in rt-PA treated Balb-C, C57BL/6, and Rabep2−/− mice, n = 10/group, */#p < 0.05, two-tailed Mann-Whitney U test.

CellPress
OPEN ACCESS
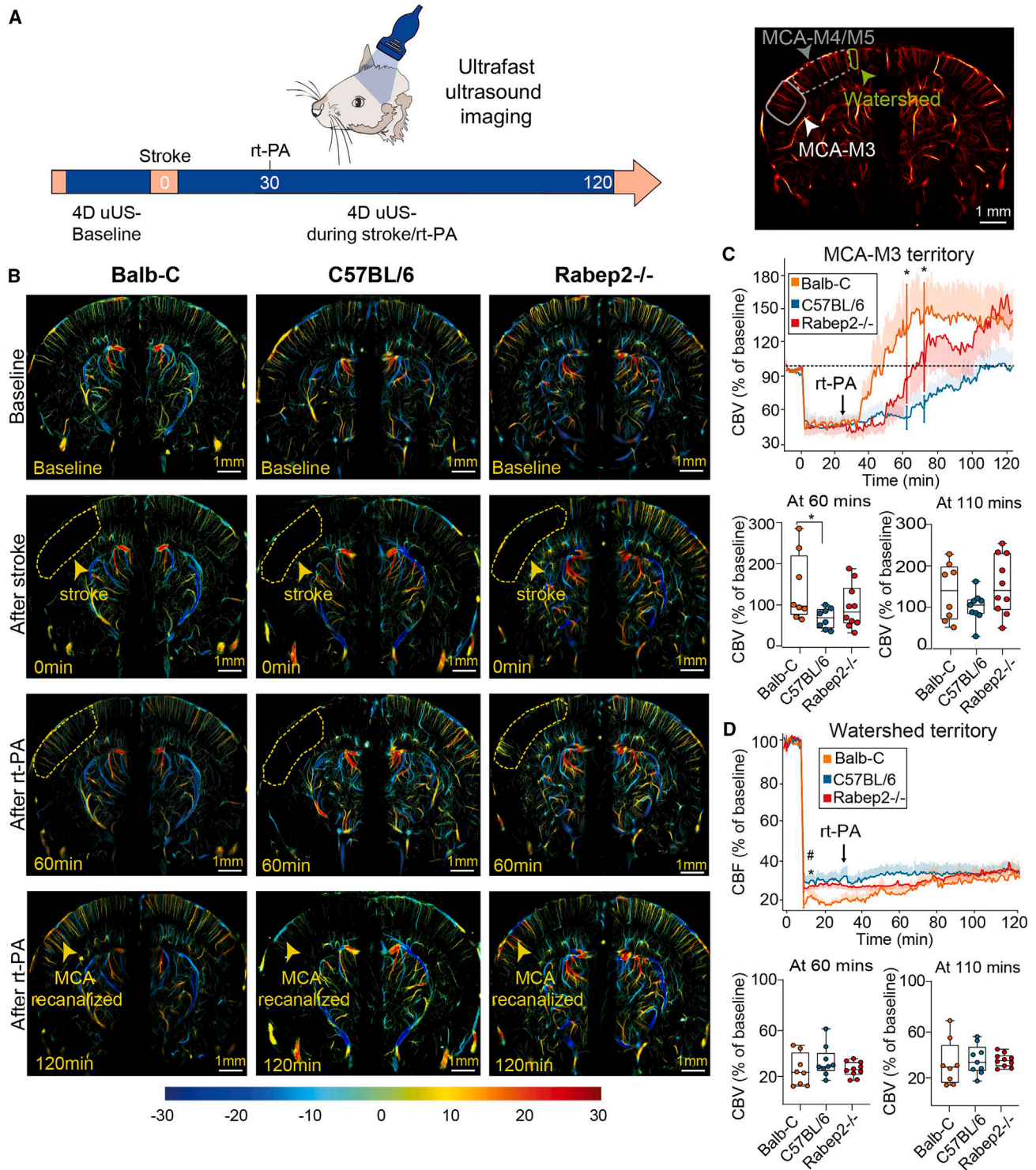
Figure 5. Reperfusion after thrombin occlusion and thrombolysis assessed by uUS

(A) Experimental setup of ultrafast ultrasound (uUS), containing 2 h post-stroke CBV monitoring (left). 3D ROI selection of the MCA-M3 and the watershed territory in view of coronal section (right).

(B) Representative 2D ULM acquisitions during baseline, immediately after stroke, 30 and 90 min after rt-PA start in Balb-C, Rabep2−/− and C57BL/6 mice. Colors indicate the flow speed in mm/s according to the color palette in the buttom.

(C and D) 4D ultrasensitive Doppler analysis of rt-PA treated Balb-C (n = 8), Rabep2−/− (n = 10) and C57BL/6 (n = 9) animals of the (C) MCA-M3 territory and the (D) watershed territory. */#p < 0.05, two-tailed Mann-Whitney U test.
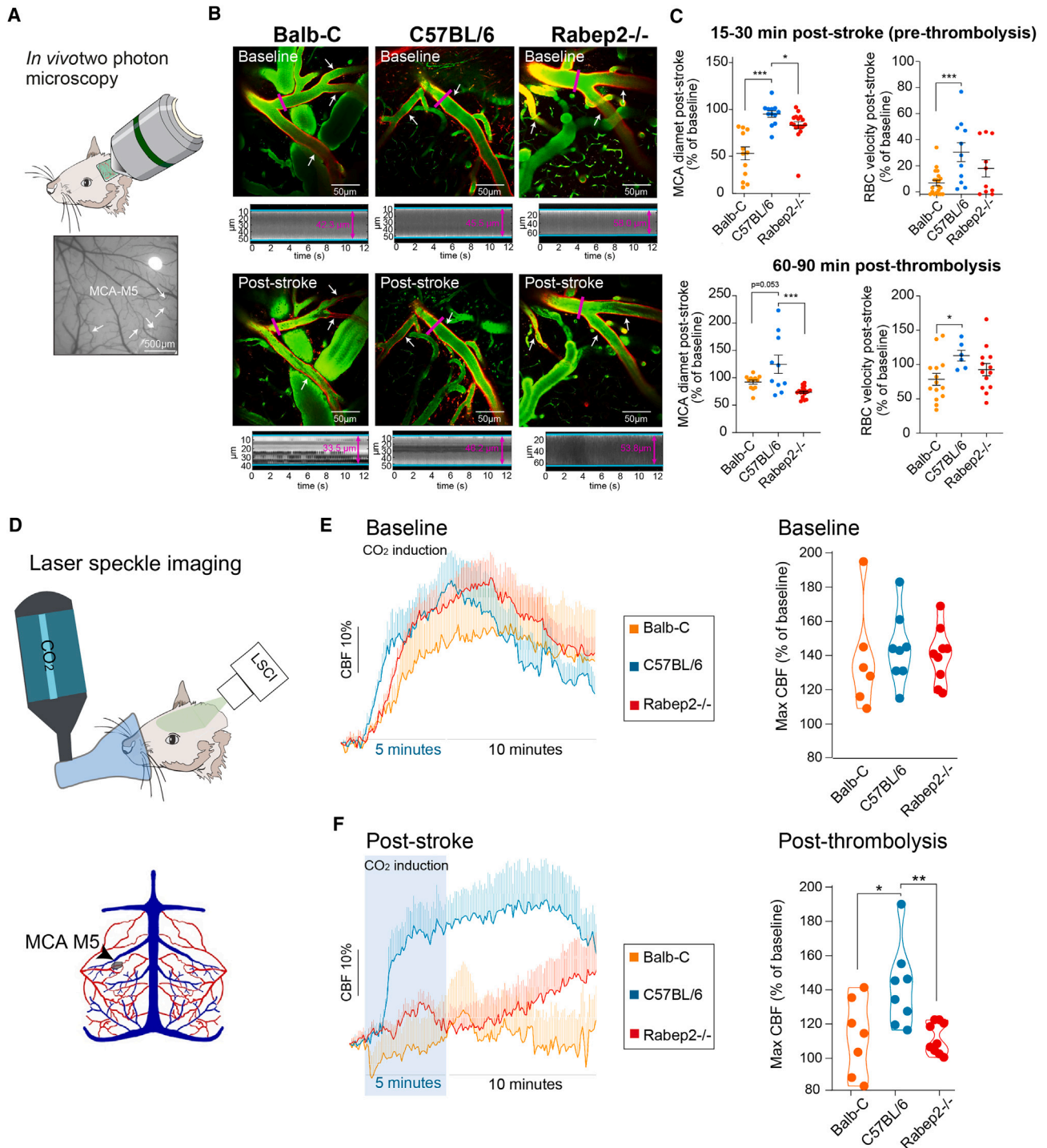
Figure 6. Vessel morphology and cerebrovascular reactivity of the MCA segments before and after stroke

(A) Cranial window of a C57BL/6 mouse. White arrowheads displaying MCA M5 segments.

(B) Representative images of distal MCA branches (white arrowheads) of Balb-C, C57BL/6, and Rabep2−/− mice pre- and post-stroke. Bottom: representative kymograph of arterial diameter changes before and after stroke.

(C) Quantification of RBC velocity and distal MCA diameter post-stroke (taken between 15 and 30 min) and post-thrombolysis (60–90 min) compared with the pre-stroke measurement (% change) is shown in n = 5 mice per strain; *p < 0.05, ***p > 0.001; two-tailed t test.

(legend continued on next page)

treatments in rodent models as well as stroke patients.[20,31,32] However, if and how collaterals affect reperfusion after stroke has remained elusive. Here, we assessed tissue perfusion and arteriole reactivity during stroke and recanalization treatment in three mouse strains with genetic-background-dependent differences in the number of native collaterals/LMCs interconnecting their MCA and ACA territories. We show that upon stroke induction, different levels of blood flow were recruited across the LMCs, depending on the number of collaterals present (i.e., "collateral status") to the ischemic territory. Infarct volume was smaller and stroke-induced functional deficits were less severe in mice with abundant LMCs. Of particular importance, we found that upon thrombolysis, poor collateral status was associated with a fast and overshooting reperfusion, culminating in more severe tissue injury and worse clinical deficit. Such pathological reperfusion response after thrombolysis in conjunction with insufficient LMCs was previously unknown. Our data from the mouse model, the *in silico* study, and from stroke patients suggest that abundant LMCs are involved in cushioning this potentially harmful reperfusion response.

Previous studies employing other stroke models of permanent vascular occlusion suggested that collaterals act as alternative routes for blood flow supply.[33–36] Our two-photon microscopy findings in the thrombin model of stroke add to this by demonstrating collateral flow and diameter increases directly after stroke, as well as a response to reperfusion treatments. Since most proximal arterial branches are not assessable by conventional imaging techniques, we used uUS (Figure 5), which can provide hemodynamic imaging of the whole brain.[37,38] By combining ultrasound with two-photon microscopy and LSCI, we established a unique picture of the dynamic changes in diameter and flow in both the collaterals themselves as well as the vessel segments in the distal MCA that they perfuse during occlusion, as well as collateral flow, vascular integrity, and reperfusion patterns from the single-vessel level to deep brain areas.

The exact mechanism of LMC regulation—if dilation is passive or if recruitment involves active mechanisms—remains largely unknown. However, in contrast to arterioles, LMCs lack myogenic responsiveness and have less SMC tone in the physiological state,[39–41] arguing against an active vasodilation during ischemia. Adding to this, under healthy conditions, almost no pressure gradient exists on the LMCs.[42] However, following occlusion of the MCA, a change in pressure causes a vasodilation, which was described previously.[43]

Based on our results, we hypothesize that by better LMC-mediated residual perfusion of the MCA endothelial cells (distal to the clot), vitality and functionality of the vessel after clot dissolution are maintained, resulting in a physiological, gradual reperfusion. By contrast, fewer LMCs and more severe hypoperfusion of the distal MCA branches during ischemia cause malfunction and decay of endothelial cells, which constrict and lose their ability to regulate reperfusion after the clot is dissolved.

In the thrombin model of stroke and thrombolysis, we observed significant differences in tissue reperfusion after recanalization. In mice with poor LMC networks, a rapid and steep CBF increase upon recanalization caused hyperperfusion of ischemic areas, hemorrhagic complications, and unfavorable outcomes. The overshoot in CBF above baseline levels observed during reperfusion in deeper, M3-supplied areas most likely resembles a loss of regulatory capacity in the affected vessels. Impaired vasodilatory capacity in response to a CO_2 stimulus in mice with poor or no LMCs confirmed this hypothesis. Thus, uncontrolled reperfusion may endanger the previously ischemic brain tissue and induce reperfusion injury.
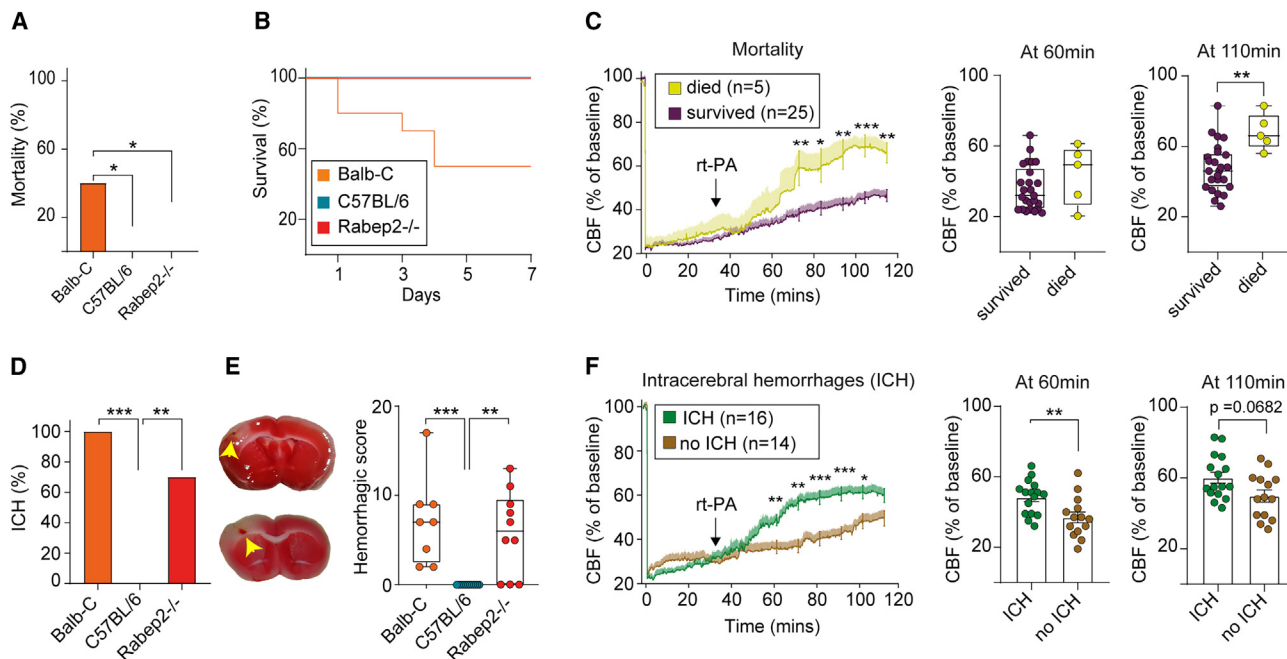
Reperfusion injury is a recognized problem in ischemic heart disease.[44] Several mechanisms have been implicated in mediating excess myocardial injury in response to coronary artery recanalization, among them mitochondrial dysfunction with the formation of reactive oxygen species, capillary and myocyte swelling, microvascular leucocyte adhesion and no reflow, as well as and increased capillary permeability.[45–47] Although ischemia in the heart and brain follow common grounds,[48] there has been no description of altered brain perfusion potentially resembling reperfusion injury in rodent models and no convincing evidence of reperfusion injury in stroke patients, so that the clinical validity of this concept was recently questioned.[49] We here provide evidence of a potentially harmful hyperemic reperfusion in stroke based on (1) dynamic flow measurements capturing hyperperfusion, (2) decomposition of vascular structures after recanalization (constriction of M5-branches on two-photon microscopy), and (3) diminished vascular function (hypercapnia challenge) in mice with poor LMCs.

Loss of vasoregulation in the recanalized MCA segment in mice with poor collaterals is likely caused by ischemic damage to vascular endothelial cells lining the lumen of arterioles and capillaries. Endothelial cells maintain vascular tone and reactivity through signals from mechanosensors, interaction with blood cells, or systemic vasoactive signals.[50] When endothelial cells undergo apoptosis and die due to stroke, this affects the vascular network as well as adjacent glial and neuronal cells.[51] LMCs can uphold residual perfusion within the ischemic region, thus protecting the vascular network and maintaining its function. Upon recanalization, when re-installation of flow forces occurs along with high pressures on the arteriolar system, gradual reperfusion maintains tissue integrity, while excessive, unregulated reperfusion accelerates tissue injury and risk of hemorrhage.

We cannot rule out that strain-specific factors other than the extent of LMC could explain differences in reperfusion patterns between Balb-C mice and the other two strains (e.g., differences in coagulation factors or individual resistance to ischemia). However, Rabep2−/− mice shared the exact same genetic

(D) Schematic drawing of hypercapnia setup (upper panel) and of the LSCI view on pial vessels and the MCA-M5 region of interest (ROI) used for analyses (lower panel).

(E and F) CBF changes before, during, and after hypercapnia during baseline (E) and 30 min after thrombolysis (F). Violin plots indicate maximal CBF increase during 15 min after CO_2 start. In n = 7 Balb-C, n = 8 C57BL/6, n = 8 Rabep2−/−; two-tailed Mann-Whitney U test.

Figure 7. Mortality and intracranial hemorrhage in Balb-C, C57BL/6 and Rabep2–/– after thrombolysis

(A and B) (A) Percentage of mortality within 7 days in rt-PA-treated Balb-C, C57BL/6, and Rabep2−/− mice (n = 10/strain) and (B) survival curve.

(C) Sub-grouped LSCI analysis of animals, which died vs. survived of all strains receiving rt-PA. *p < 0.05, **p < 0.01; ***p < 0.001, two-tailed Mann-Whitney U test.

(D–F) Intracranial hemorrhage (ICH) assessment.

(D) Overall percentage of rt-PA treated animals showing ICHs plus representative TTC image on day 7.

(E) Quantifications of hemorrhages (yellow arrows). The hemorrhagic score contains microscopic and macroscopic assessment.[7] **p < 0.01; ***p < 0.001, two-tailed t test.

(F) Sub-grouping of LSCIs of rt-PA treated mice that showed ICHs vs. mice without; *p < 0.05, **p < 0.01; ***p < 0.001, two-tailed Mann-Whitney U test.

background compared with C57BL/6 mice except for the mutant gene Rabep2, arguing against other variables significantly affecting the observed difference in reperfusion response. The point mutation in the Rabep2 gene within the *Dce1* locus on chromosome 7 does not affect microvessel or capillary density in these mice.[17] This is further supported by data obtained from the Rabep2 +/+ littermates. Moreover, by using microvascular networks that only differ in the extent of LMCs, the *in silico* study confirms that the number of LMCs matters for the level of flow recruitment during stroke. In our model, recanalization success was independent of LMC status. The thrombin model is a clinically relevant model of stroke, clot formation, and lysis as well as vascular responses to intravenous thrombolysis, using the same rt-PA dose and infusion rate as in patients. Other animal models of stroke using filaments, ligatures, clamping, or electrocoagulation do not capture the processes involved in the recanalization of a clot and thrombolysis-induced reperfusion.[52–54] Although extent of collaterals was previously shown to correlate with thrombus length[55] and fibrinolysis resistance,[56] our model with very fresh and homogenous clots may not reflect heterogeneity in clot composition and source present in stroke patients. However, thus, we were able to observe reperfusion dynamics in relation to collateral status independent of clot composition.
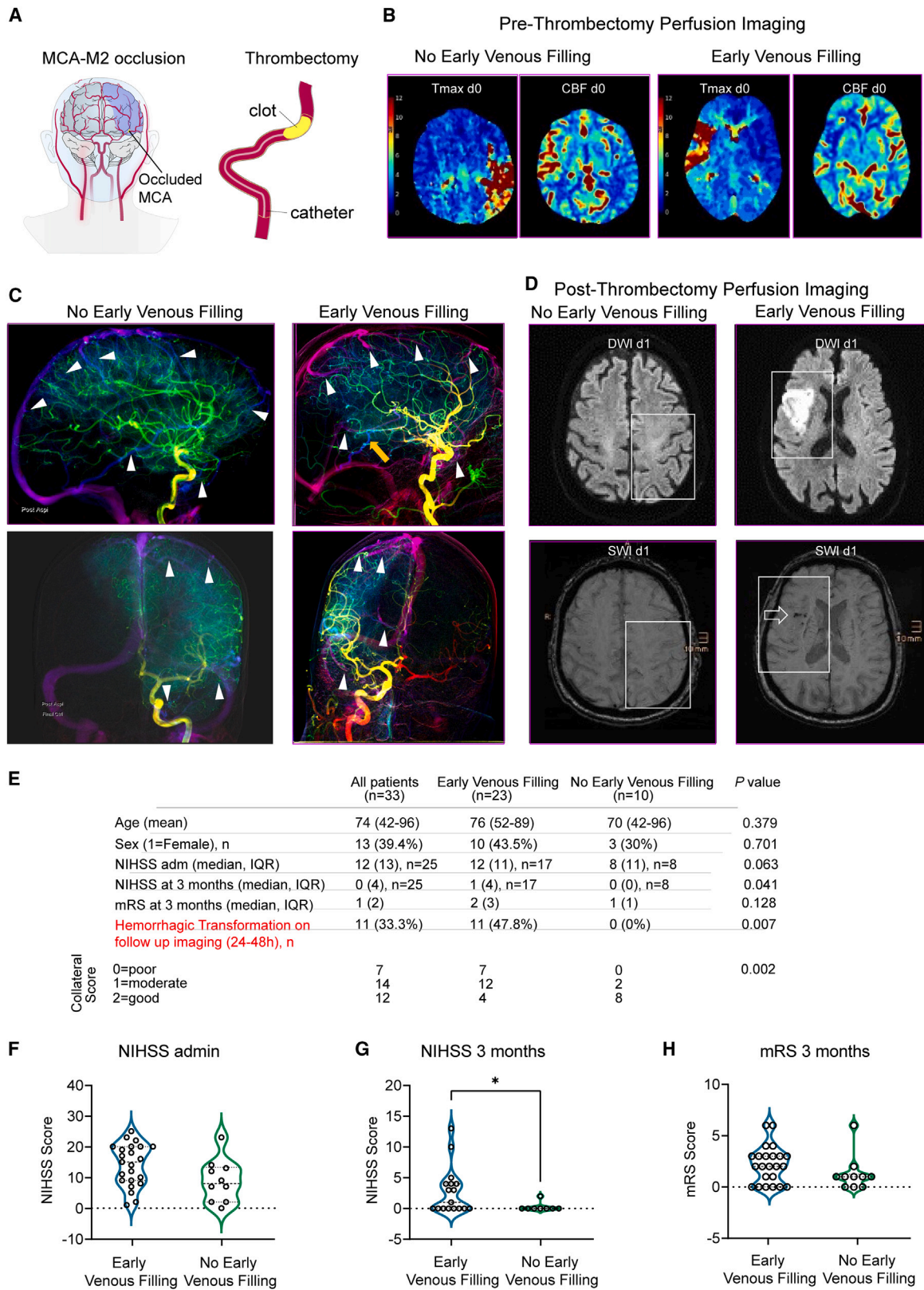
Strikingly, we demonstrated a similar rapid reperfusion pattern in patients with poor collaterals and ischemic stroke who had un-

dergone recanalization through thrombectomy. We used color-coding according to DSA contrast arrival times directly post-thrombectomy in patients with stroke due to distal MCA-M1 or MCA-M2 occlusion. Early venous filling, albeit investigated with a different analysis approach and in a more heterogeneous stroke patient cohort, was previously suggested to indicate harmful hyperperfusion following thrombectomy.[57,58]

In our patient cohort, this was reflected by more severe neurological deficits (NIHSS) at 3 months and hemorrhagic transformations of the infarcted area on follow-up imaging. Hemorrhages on SWI-MRI are indicators of blood-brain-barrier disruption, one of the hallmarks of secondary infarct complications.[59] Therefore, early venous filling may indicate patients at risk of ICH and futile recanalization immediately post-thrombectomy, thus calling for intensive post-interventional medical monitoring.

Our findings have important implications for stroke treatment. LMCs are crucial for preventing reperfusion injury arising from recanalization. We show that patients with poor LMCs are more likely to suffer from a severe stroke due to a lack of compensatory intra-ischemic perfusion. After detecting CBF patterns with advanced imaging techniques, this study strengthens the proposition that LMC status should be taken into account as an indicator of vulnerable stroke patients.[60] Importantly, we demonstrate that patients with poor LMCs are at particular risk of rapid reperfusion associated with more

CellPress
OPEN ACCESS

A MCA-M2 occlusion / Thrombectomy

B Pre-Thrombectomy Perfusion Imaging
No Early Venous Filling — Tmax d0, CBF d0
Early Venous Filling — Tmax d0, CBF d0

C No Early Venous Filling / Early Venous Filling

D Post-Thrombectomy Perfusion Imaging
No Early Venous Filling — DWI d1, SWI d1
Early Venous Filling — DWI d1, SWI d1

E

	All patients (n=33)	Early Venous Filling (n=23)	No Early Venous Filling (n=10)	P value
Age (mean)	74 (42-96)	76 (52-89)	70 (42-96)	0.379
Sex (1=Female), n	13 (39.4%)	10 (43.5%)	3 (30%)	0.701
NIHSS adm (median, IQR)	12 (13), n=25	12 (11), n=17	8 (11), n=8	0.063
NIHSS at 3 months (median, IQR)	0 (4), n=25	1 (4), n=17	0 (0), n=8	0.041
mRS at 3 months (median, IQR)	1 (2)	2 (3)	1 (1)	0.128
Hemorrhagic Transformation on follow up imaging (24-48h), n	11 (33.3%)	11 (47.8%)	0 (0%)	0.007
Collateral Score 0=poor	7	7	0	0.002
1=moderate	14	12	2	
2=good	12	4	8	

F NIHSS admin — NIHSS Score — Early Venous Filling / No Early Venous Filling

G NIHSS 3 months — NIHSS Score — Early Venous Filling / No Early Venous Filling *

H mRS 3 months — mRS Score — Early Venous Filling / No Early Venous Filling

(legend on next page)

CellPress
OPEN ACCESS

Neuron
Article

severe tissue damage and hemorrhagic infarct transformation after stroke treatments, which should be considered in stroke trials. Longer times to treatment could be exceedingly dangerous in these patients. Vascular risk factors are likely to affect LMC function, which should be investigated further. In addition to their potential use as biomarkers for outcome of stroke treatments, LMCs may be targeted for stroke treatments. In the IMPACT 24 trial, flow increase in ipsilateral collaterals induced by sphenopalatine ganglion stimulation showed promising results for stroke patients with cortical stroke in the anterior circulation.[61] In addition to fostering LMC function through adjunctive protective therapies, another potential approach could be slowing down rapid reperfusion (e.g., by graded or staccato removal of the obstructive clot in patients with poor LMCs), thus reducing tissue injury and improving stroke patient outcome.

STAR★METHODS

Detailed methods are provided in the online version of this paper and include the following:

- KEY RESOURCES TABLE
- RESOURCE AVAILABILITY
  ○ Lead contact
  ○ Materials availability
  ○ Data and code availability
- EXPERIMENTAL MODEL AND STUDY PARTICIPANT DETAILS
  ○ Animals
  ○ Humans
- METHOD DETAILS
  ○ Anaesthesia
  ○ Head-Post Implantation
  ○ Cranial window surgery
  ○ Thrombin stroke model
  ○ Rt-PA administration
  ○ Laser Speckle Cortical Imaging (LSCI)
  ○ Two-photon imaging
  ○ Ultrafast ultrasound imaging
  ○ 4D Ultrasensitive Doppler
  ○ Automatic probe positioning
  ○ Data processing
  ○ Vascular Territories (VT) segmentation and CBV time-profile extraction
  ○ Ultrasound Localization Microscopy

  ○ CO_2 challenge
  ○ Tissue clearing
  ○ Whole-brain imaging
  ○ Quantification of lesion volume and hemorrhages
  ○ Behavioral assessment
  ○ In-silico model
  ○ DSA data analysis
- QUANTIFICATION AND STATISTICAL ANALYSIS

SUPPLEMENTAL INFORMATION

Supplemental information can be found online at https://doi.org/10.1016/j.neuron.2024.01.031.

AUTHOR CONTRIBUTIONS

Conceptualization, N.F.B., M.E.A., and S.W.; methodology, M.E.A., A.M.R., A.B., P.T., T.D., N.F.B., C.G., P.B., Z.K., M.T., D.V., M.T.W., C.L., R.E., F.S., and B.W.; investigation, N.F.B., C.G., W.M., A.B., P.T., D.F., H.-L.H., P.B., C.L., R.E., F.S., S.W., and M.E.A.; writing – original draft, N.F.B., M.E.A., F.S., and S.W.; writing – review & editing, all; funding acquisition, S.W., M.E.A., A.L., M.W., A.A., B.W., and F.S.; resources, S.W., M.W., B.W., D.V., and M.T.; supervision, M.E.A., T.D., M.W., C.O., Z.K., M.T., D.V., F.S., B.W., and S.W.

DECLARATION OF INTERESTS

The authors declare no competing interests.

REFERENCES

1. Virani, S.S., Alonso, A., Aparicio, H.J., Benjamin, E.J., Bittencourt, M.S., Callaway, C.W., Carson, A.P., Chamberlain, A.M., Cheng, S., Delling, F.N., et al. (2021). Heart disease and stroke Statistics-2021 update: A report from the American Heart Association. Circulation *143*, e254–e743.

Figure 8. Rapid reperfusion after thrombectomy in stroke patients
(A) Schematic representation of the location of MCA-M2 occlusion in stroke patients.
(B) Pre-thrombectomy CT perfusion imaging in two stroke patients with distal MCA-M1 occlusion. Both have similar extent and severity of the perfusion deficit on Tmax maps (a Tmax > 6 s corresponds to the ischemic core area), and corresponding CBF maps. Left patient (MCA-M2 occlusion on the left) had no early venous filling post-thrombectomy, right patient MCA-M2 occlusion the right) showed early venous filling after thrombectomy.
(C) Color-coded MIP (maximum intensity projection) DSA data from a patient without (left) and with (right) early venous filling indicated using white arrowheads.
(D) MRI 1 day after thrombectomy from the same two patients as in (B) shows early infarct extension on diffusion-weighted images (DWI; white area) within the former hypoperfused area (white box). Below: corresponding slice from Susceptibility Weighted Image (SWI), where blood deposits appear black (arrow on the right side). Note that the patient with early venous filling has a considerably larger infarct on DWI and hemorrhagic transformation on SWI.
(E) Patient characteristics.
(F–H) Violin plots with individual values of NIHSS data (F) on admin, (G) after 3 months, and (H) mRS scores 3 months after stroke; *p < 0.05, two-tailed Mann-Whitney U test.

Neuron
Article

CellPress
OPEN ACCESS

2. Campbell, B.C.V., De Silva, D.A., Macleod, M.R., Coutts, S.B., Schwamm, L.H., Davis, S.M., and Donnan, G.A. (2019). Ischaemic stroke. Nat. Rev. Dis. Primers 5, 70.

3. Espinosa de Rueda, M., Parrilla, G., Manzano-Fernández, S., García-Villalba, B., Zamarro, J., Hernández-Fernández, F., Sánchez-Vizcaino, C., Carreón, E., Morales, A., and Moreno, A. (2015). Combined multimodal computed tomography score correlates with futile recanalization after thrombectomy in patients with acute stroke. Stroke 46, 2517–2522.

4. Goyal, M., Menon, B.K., van Zwam, W.H., Dippel, D.W., Mitchell, P.J., Demchuk, A.M., Dávalos, A., Majoie, C.B., van der Lugt, A., de Miquel, M.A., et al. (2016). Endovascular thrombectomy after large-vessel ischaemic stroke: a meta-analysis of individual patient data from five randomised trials. Lancet 387, 1723–1731.

5. Wong, G.J., Yoo, B., Liebeskind, D., Baharvahdat, H., Gornbein, J., Jahan, R., Szeder, V., Duckwiler, G., Tateshima, S., Colby, G., et al. (2021). Frequency, determinants, and outcomes of emboli to distal and new territories related to mechanical thrombectomy for acute ischemic stroke. Stroke 52, 2241–2249.

6. Yemisci, M., Gursoy-Ozdemir, Y., Vural, A., Can, A., Topalkara, K., and Dalkara, T. (2009). Pericyte contraction induced by oxidative-nitrative stress impairs capillary reflow despite successful opening of an occluded cerebral artery. Nat. Med. 15, 1031–1037.

7. El Amki, M., Glück, C., Binder, N., Middleham, W., Wyss, M.T., Weiss, T., Meister, H., Luft, A., Weller, M., Weber, B., and Wegener, S. (2020). Neutrophils obstructing brain capillaries are a major cause of no-reflow in ischemic stroke. Cell Rep. 33, 108260.

8. Stoll, G., and Pham, M. (2020). Beyond recanalization - a call for action in acute stroke. Nat. Rev. Neurol. 16, 591–592.

9. Liebeskind, D.S. (2003). Collateral circulation. Stroke 34, 2279–2284.

10. Schaper, W. (2009). Collateral circulation: past and present. Basic Res. Cardiol. 104, 5–21.

11. Romero, J.R., Pikula, A., Nguyen, T.N., Nien, Y.L., Norbash, A., and Babikian, V.L. (2009). Cerebral collateral circulation in carotid artery disease. Curr. Cardiol. Rev. 5, 279–288.

12. Epp, R., Glück, C., Binder, N.F., El Amki, M., Weber, B., Wegener, S., Jenny, P., and Schmid, F. (2023). The role of leptomeningeal collaterals in redistributing blood flow during stroke. PLoS Comput. Biol. 19, e1011496.

13. Faber, J.E., Storz, J.F., Cheviron, Z.A., and Zhang, H. (2021). High-altitude rodents have abundant collaterals that protect against tissue injury after cerebral, coronary and peripheral artery occlusion. J. Cereb. Blood Flow Metab. 41, 731–744.

14. Liebeskind, D.S., Saber, H., Xiang, B., Jadhav, A.P., Jovin, T.G., Haussen, D.C., Budzik, R.F., Bonafe, A., Bhuva, P., Yavagal, D.R., et al. (2022). Collateral circulation in thrombectomy for stroke after 6 to 24 hours in the DAWN trial. Stroke 53, 742–748.

15. García-Tornel, Á., Ciolli, L., Rubiera, M., Requena, M., Muchada, M., Pagola, J., Rodriguez-Luna, D., Deck, M., Juega, J., Rodríguez-Villatoro, N., et al. (2021). Leptomeningeal collateral flow modifies endovascular treatment efficacy on large-vessel occlusion strokes. Stroke 52, 299–303.

16. Schuler, F., Rotkopf, L.T., Apel, D., Fabritius, M.P., Tiedt, S., Wollenweber, F.A., Kellert, L., Dorn, F., Liebig, T., Thierfelder, K.M., and Kunz, W.G. (2020). Differential benefit of collaterals for stroke patients treated with thrombolysis or supportive care: A propensity score matched analysis. Clin. Neuroradiol. 30, 525–533.

17. Lucitti, J.L., Sealock, R., Buckley, B.K., Zhang, H., Xiao, L., Dudley, A.C., and Faber, J.E. (2016). Variants of Rab GTPase-effector binding Protein-2 cause variation in the collateral circulation and severity of stroke. Stroke 47, 3022–3031.

18. Chalothorn, D., Clayton, J.A., Zhang, H., Pomp, D., and Faber, J.E. (2007). Collateral density, remodeling, and VEGF-A expression differ widely between mouse strains. Physiol. Genomics 30, 179–191.

19. Zhang, H., Prabhakar, P., Sealock, R., and Faber, J.E. (2010). Wide genetic variation in the native pial collateral circulation is a major determinant of variation in severity of stroke. J. Cereb. Blood Flow Metab. 30, 923–934.

20. Zhang, H., and Faber, J.E. (2019). Transient versus Permanent MCA Occlusion in Mice Genetically Modified to Have Good versus Poor Collaterals. Med One 4, e190024.

21. Renier, N., Wu, Z., Simon, D.J., Yang, J., Ariel, P., and Tessier-Lavigne, M. (2014). iDISCO: a simple, rapid method to immunolabel large tissue samples for volume imaging. Cell 159, 896–910.

22. Kirst, C., Skriabine, S., Vieites-Prado, A., Topilko, T., Bertin, P., Gerschenfeld, G., Verny, F., Topilko, P., Michalski, N., Tessier-Lavigne, M., and Renier, N. (2020). Mapping the fine-scale organization and plasticity of the brain vasculature. Cell 180, 780–795.e25.

23. El Amki, M., Lerouet, D., Coqueran, B., Curis, E., Orset, C., Vivien, D., Plotkine, M., Marchand-Leroux, C., and Margaill, I. (2012). Experimental modeling of recombinant tissue plasminogen activator effects after ischemic stroke. Exp. Neurol. 238, 138–144.

24. Orset, C., Macrez, R., Young, A.R., Panthou, D., Angles-Cano, E., Maubert, E., Agin, V., and Vivien, D. (2007). Mouse model of in situ thromboembolic stroke and reperfusion. Stroke 38, 2771–2778.

25. Davis, M.A., Kazmi, S.M., and Dunn, A.K. (2014). Imaging depth and multiple scattering in laser speckle contrast imaging. J. Biomed. Opt. 19, 086001.

26. Deffieux, T., Demené, C., and Tanter, M. (2021). Functional ultrasound imaging: A new imaging modality for neuroscience. Neuroscience 474, 110–121.

27. Zaidat, O.O., Yoo, A.J., Khatri, P., Tomsick, T.A., von Kummer, R., Saver, J.L., Marks, M.P., Prabhakaran, S., Kallmes, D.F., Fitzsimmons, B.F., et al. (2013). Recommendations on angiographic revascularization grading standards for acute ischemic stroke: a consensus statement. Stroke 44, 2650–2663.

28. Deng, G., Xiao, J., Yu, H., Chen, M., Shang, K., Qin, C., and Tian, D.S. (2022). Predictors of futile recanalization after endovascular treatment in acute ischemic stroke: a meta-analysis. J. Neurointerv Surg. 14, 881–885.

29. Hossmann, K.A. (1994). Viability thresholds and the penumbra of focal ischemia. Ann. Neurol. 36, 557–565.

30. Eltzschig, H.K., and Eckle, T. (2011). Ischemia and reperfusion–from mechanism to translation. Nat. Med. 17, 1391–1401.

31. Lee, H.K., Kwon, D.H., Aylor, D.L., and Marchuk, D.A. (2022). A cross-species approach using an in vivo evaluation platform in mice demonstrates that sequence variation in human RABEP2 modulates ischemic stroke outcomes. Am. J. Hum. Genet. 109, 1814–1827.

32. Maguida, G., and Shuaib, A. (2023). Collateral circulation in ischemic stroke: an updated review. J. Stroke 25, 179–198.

33. Schaffer, C.B., Friedman, B., Nishimura, N., Schroeder, L.F., Tsai, P.S., Ebner, F.F., Lyden, P.D., and Kleinfeld, D. (2006). Two-photon imaging of cortical surface microvessels reveals a robust redistribution in blood flow after vascular occlusion. PLoS Biol. 4, e22.

34. Ma, J., Ma, Y., Shuaib, A., and Winship, I.R. (2020). Improved collateral flow and reduced damage after remote ischemic perconditioning during distal middle cerebral artery occlusion in aged rats. Sci. Rep. 10, 12392.

35. Kanoke, A., Akamatsu, Y., Nishijima, Y., To, E., Lee, C.C., Li, Y., Wang, R.K., Tominaga, T., and Liu, J. (2020). The impact of native leptomeningeal collateralization on rapid blood flow recruitment following ischemic stroke. J. Cereb. Blood Flow Metab. 40, 2165–2178.

36. Ma, J., Ma, Y., Shuaib, A., and Winship, I.R. (2020). Impaired collateral flow in pial arterioles of aged rats during ischemic stroke. Transl. Stroke Res. 11, 243–253.

37. Errico, C., Pierre, J., Pezet, S., Desailly, Y., Lenkei, Z., Couture, O., and Tanter, M. (2015). Ultrafast ultrasound localization microscopy for deep super-resolution vascular imaging. Nature 527, 499–502.

38. Renaudin, N., Demené, C., Dizeux, A., Ialy-Radio, N., Pezet, S., and Tanter, M. (2022). Functional ultrasound localization microscopy reveals

brain-wide neurovascular activity on a microscopic scale. Nat. Methods *19*, 1004–1012.

39. Beard, D.J., Murtha, L.A., McLeod, D.D., and Spratt, N.J. (2016). Intracranial pressure and collateral blood flow. Stroke *47*, 1695–1700.

40. Chan, S.L., Sweet, J.G., Bishop, N., and Cipolla, M.J. (2016). Pial collateral reactivity during hypertension and aging: understanding the function of collaterals for stroke therapy. Stroke *47*, 1618–1625.

41. Zhang, H., Chalothorn, D., and Faber, J.E. (2019). Collateral vessels have unique endothelial and smooth muscle cell phenotypes. Int. J. Mol. Sci. *20*, 3608.

42. Chalothorn, D., and Faber, J.E. (2010). Formation and maturation of the native cerebral collateral circulation. J. Mol. Cell. Cardiol. *49*, 251–259.

43. Buschmann, I., and Schaper, W. (2000). The pathophysiology of the collateral circulation (arteriogenesis). J. Pathol. *190*, 338–342.

44. Heusch, G., and Gersh, B.J. (2017). The pathophysiology of acute myocardial infarction and strategies of protection beyond reperfusion: a continual challenge. Eur. Heart J. *38*, 774–784.

45. Zhou, M., Yu, Y., Luo, X., Wang, J., Lan, X., Liu, P., Feng, Y., and Jian, W. (2021). Myocardial ischemia-reperfusion injury: therapeutics from a mitochondria-centric perspective. Cardiology *146*, 781–792.

46. Yellon, D.M., and Hausenloy, D.J. (2007). Myocardial reperfusion injury. N. Engl. J. Med. *357*, 1121–1135.

47. García-Prieto, J., Villena-Gutiérrez, R., Gómez, M., Bernardo, E., Pun-García, A., García-Lunar, I., Crainiciuc, G., Fernández-Jiménez, R., Sreeramkumar, V., Bourio-Martínez, R., et al. (2017). Neutrophil stunning by metoprolol reduces infarct size. Nat. Commun. *8*, 14780.

48. Kloner, R.A., King, K.S., and Harrington, M.G. (2018). No-reflow phenomenon in the heart and brain. Am. J. Physiol. Heart Circ. Physiol. *315*, H550–H562.

49. Gauberti, M., Lapergue, B., Martinez de Lizarrondo, S., Vivien, D., Richard, S., Bracard, S., Piotin, M., and Gory, B. (2018). Ischemia-reperfusion injury after endovascular thrombectomy for ischemic stroke. Stroke *49*, 3071–3074.

50. Ashby, J.W., and Mack, J.J. (2021). Endothelial control of cerebral blood flow. Am. J. Pathol. *191*, 1906–1916.

51. Zille, M., Ikhsan, M., Jiang, Y., Lampe, J., Wenzel, J., and Schwaninger, M. (2019). The impact of endothelial cell death in the brain and its role after stroke: A systematic review. Cell Stress *3*, 330–347.

52. Carmichael, S.T. (2005). Rodent models of focal stroke: size, mechanism, and purpose. Neurorx *2*, 396–409.

53. Doyle, K.P., and Buckwalter, M.S. (2014). A mouse model of permanent focal ischemia: distal middle cerebral artery occlusion. Methods Mol. Biol. *1135*, 103–110.

54. Chauveau, F., Moucharrafie, S., Wiart, M., Brisset, J.C., Berthezène, Y., Nighoghossian, N., and Cho, T.H. (2010). In vivo MRI assessment of permanent middle cerebral artery occlusion by electrocoagulation: pitfalls of procedure. Exp. Transl. Stroke Med. *2*, 4.

55. Qazi, E.M., Sohn, S.I., Mishra, S., Almekhlafi, M.A., Eesa, M., d'Esterre, C.D., Qazi, A.A., Puig, J., Goyal, M., Demchuk, A.M., and Menon, B.K. (2015). Thrombus characteristics are related to collaterals and angioarchitecture in acute stroke. Can. J. Neurol. Sci. *42*, 381–388.

56. Seners, P., Roca, P., Legrand, L., Turc, G., Cottier, J.P., Cho, T.H., Arquizan, C., Bracard, S., Ozsancak, C., Ben Hassen, W., et al. (2019). Better collaterals are independently associated with post-thrombolysis recanalization before thrombectomy. Stroke *50*, 867–872.

57. Shimonaga, K., Matsushige, T., Takahashi, H., Hashimoto, Y., Mizoue, T., Ono, C., Kurisu, K., and Sakamoto, S. (2020). Early venous filling after reperfusion therapy in acute ischemic stroke. J. Stroke Cerebrovasc. Dis. *29*, 104926.

58. Janvier, P., Kerleroux, B., Turc, G., Pasi, M., Farhat, W., Bricout, N., Benzakoun, J., Legrand, L., Clarençon, F., Bracard, S., et al. (2022). TAGE score for symptomatic intracranial hemorrhage prediction after successful endovascular treatment in acute ischemic stroke. Stroke *53*, 2809–2817.

59. Zhao, G., Sun, L., Wang, Z., Wang, L., Cheng, Z., Lei, H., Yang, D., Cui, Y., and Zhang, S. (2017). Evaluation of the role of susceptibility-weighted imaging in thrombolytic therapy for acute ischemic stroke. J. Clin. Neurosci. *40*, 175–179.

60. Shuaib, A., Butcher, K., Mohammad, A.A., Saqqur, M., and Liebeskind, D.S. (2011). Collateral blood vessels in acute ischaemic stroke: a potential therapeutic target. Lancet Neurol. *10*, 909–921.

61. Bornstein, N.M., Saver, J.L., Diener, H.C., Gorelick, P.B., Shuaib, A., Solberg, Y., Thackeray, L., Savic, M., Janelidze, T., Zarqua, N., et al. (2019). An injectable implant to stimulate the sphenopalatine ganglion for treatment of acute ischaemic stroke up to 24 h from onset (ImpACT-24B): an international, randomised, double-blind, sham-controlled, pivotal trial. Lancet *394*, 219–229.

62. Pologruto, T.A., Sabatini, B.L., and Svoboda, K. (2003). ScanImage: flexible software for operating laser scanning microscopes. Biomed. Eng. OnLine *2*, 13.

63. Schmid, F., Barrett, M.J.P., Obrist, D., Weber, B., and Jenny, P. (2019). Red blood cells stabilize flow in brain microvascular networks. PLoS Comput. Biol. *15*, e1007231.

64. Lyden, P., Brott, T., Tilley, B., Welch, K.M., Mascha, E.J., Levine, S., Haley, E.C., Grotta, J., and Marler, J. (1994). Improved reliability of the NIH Stroke Scale using video training. NINDS TPA Stroke Study Group. Stroke *25*, 2220–2226.

65. Banks, J.L., and Marotta, C.A. (2007). Outcomes validity and reliability of the modified Rankin scale: implications for stroke clinical trials: a literature review and synthesis. Stroke *38*, 1091–1096.

66. Campbell, B.C., Mitchell, P.J., Kleinig, T.J., Dewey, H.M., Churilov, L., Yassi, N., Yan, B., Dowling, R.J., Parsons, M.W., Oxley, T.J., et al. (2015). Endovascular therapy for ischemic stroke with perfusion-imaging selection. N. Engl. J. Med. *372*, 1009–1018.

67. Holtmaat, A., Bonhoeffer, T., Chow, D.K., Chuckowree, J., De Paola, V., Hofer, S.B., Hübener, M., Keck, T., Knott, G., Lee, W.C., et al. (2009). Long-term, high-resolution imaging in the mouse neocortex through a chronic cranial window. Nat. Protoc. *4*, 1128–1144.

68. El Amki, M., Lerouet, D., Garraud, M., Teng, F., Beray-Berthat, V., Coqueran, B., Barsacq, B., Abbou, C., Palmier, B., Marchand-Leroux, C., and Margaill, I. (2018). Improved reperfusion and vasculoprotection by the poly(ADP-ribose)polymerase inhibitor PJ34 after stroke and thrombolysis in mice. Mol. Neurobiol. *55*, 9156–9168.

69. Sekhon, L.H., Spence, I., Morgan, M.K., and Weber, N.C. (1995). Chronic cerebral hypoperfusion in the rat: temporal delineation of effects and the in vitro ischemic threshold. Brain Res. *704*, 107–111.

70. Maysami, S., Wong, R., Pradillo, J.M., Denes, A., Dhungana, H., Malm, T., Koistinaho, J., Orset, C., Rahman, M., Rubio, M., et al. (2016). A cross-laboratory preclinical study on the effectiveness of interleukin-1 receptor antagonist in stroke. J. Cereb. Blood Flow Metab. *36*, 596–605.

71. Mayrhofer, J.M., Haiss, F., Haenni, D., Weber, S., Zuend, M., Barrett, M.J., Ferrari, K.D., Maechler, P., Saab, A.S., Stobart, J.L., et al. (2015). Design and performance of an ultra-flexible two-photon microscope for in vivo research. Biomed. Opt. Express *6*, 4228–4237.

72. Nouhoum, M., Ferrier, J., Osmanski, B.F., Ialy-Radio, N., Pezet, S., Tanter, M., and Deffieux, T. (2021). A functional ultrasound brain GPS for automatic vascular-based neuronavigation. Sci. Rep. *11*, 15197.

73. Voigt, F.F., Kirschenbaum, D., Platonova, E., Pagès, S., Campbell, R.A.A., Kastli, R., Schaettin, M., Egolf, L., van der Bourg, A., Bethge, P., et al. (2019). The mesoSPIM initiative: open-source light-sheet microscopes for imaging cleared tissue. Nat. Methods *16*, 1105–1108.

74. El Amki, M., Binder, N., Steffen, R., Schneider, H., Luft, A.R., Weller, M., Imthurn, B., Merki-Feld, G.S., and Wegener, S. (2019). Contraceptive drugs mitigate experimental stroke-induced brain injury. Cardiovasc. Res. *115*, 637–646.

Neuron
Article

75. Haddad, M., Beray-Berthat, V., Coqueran, B., Palmier, B., Szabo, C., Plotkine, M., and Margaill, I. (2008). Reduction of hemorrhagic transformation by PJ34, a poly(ADP-ribose)polymerase inhibitor, after permanent focal cerebral ischemia in mice. Eur. J. Pharmacol. *588*, 52–57.

76. Wahl, F., Allix, M., Plotkine, M., and Boulu, R.G. (1992). Neurological and behavioral outcomes of focal cerebral ischemia in rats. Stroke *23*, 267–272.

77. Schmid, F., Tsai, P.S., Kleinfeld, D., Jenny, P., and Weber, B. (2017). Depth-dependent flow and pressure characteristics in cortical microvascular networks. PLoS Comput. Biol. *13*, e1005392.

78. Pries, A.R., Secomb, T.W., Gaehtgens, P., and Gross, J.F. (1990). Blood flow in microvascular networks. Experiments and simulation. Circ. Res. *67*, 826–834.

CellPress
OPEN ACCESS

Neuron
Article

STAR★METHODS

KEY RESOURCES TABLE

REAGENT or RESOURCE	SOURCE	IDENTIFIER
Antibodies		
Anti-α-smooth muscle actin	Sigma Aldrich	Cat #C6198
Chemicals, peptides, and recombinant proteins		
Fentanyl	Sintetica	Cat #699811
Midazolam	Roche	Cat #M-908-1ML
Medetomidine	Orion Pharma	Cat #520370
Buprenorphine	Sintetica	
Human alpha-thrombin	Haematologic Techn.	Cat #HCT-0020
2,3,5-triphenyltetrazolium chloride	Sigma-Aldrich	Cat. #T8877
Actilyse® rt-PA	Boehringer Ingelheim	
FITC-dextrane	Sigma-Aldrich	FD2000S
Hydrazide (Alexa Fluor™ 633)	Hydrazide Life Technologies	Cat. #A30634
Texas red Dextran	Life Technologies	Cat #D-1864
Experimental models: Organisms/strains		
C57BL/6	Charles Rivers	Cat #000664
Rabep2-/-	The Jackson Laboratories	Cat #029463
BALB/C mice	Charles Rivers	Cat #028
Human participants.	This paper	N/A
Software and algorithms		
CHIPS toolbox for MATLAB	GitHub	https://github.com/EIN-lab/CHIPS
ImageJ version 1.8.0_172 64 bit	ImageJ Software	https://imagej.nih.gov/
IBM SPSS Statistics (Version 27, 28)	SPSS Software	https://www.ibm.com/spss
ART	Inserm U1273, Paris, France & Iconeus	https://www.physicsformedicine.espci.fr/technology-transfer/art
ScanImage	Pologruto et al[62]	N/A
Radon algorithm	Schmid et al.[63]	N/A
MATLAB	Mathworks	https://www.mathworks.com/products/matlab.html
Imaris	Oxford instruments, 9.8.0	https://imaris.oxinst.com/
GraphPad Prism v8.0	GraphPad Software	https://www.graphpad.com/

RESOURCE AVAILABILITY

Lead contact
Further information and requests for resources and reagents should be directed to and will be fulfilled by the lead contact, Susanne Wegener (susanne.wegener@usz.ch).

Materials availability
This study did not generate any new unique reagents.

Data and code availability
- All data reported in this paper will be shared by the lead contact upon request.
- This study does not report original code.
- Any additional information required to reanalyze the data reported in this paper is available from the lead contact upon request.

EXPERIMENTAL MODEL AND STUDY PARTICIPANT DETAILS

Animals

For all experiments, Balb-C (Charles Rivers, no. 028), C57BL/6 (Charles Rivers, no. 000664) and Rabep2-/-[17] mice, mixed female/male, between 3 to 4 months of age were used. There was no influence/association of sex on the findings. The animals had free access to water and food and an inverted 12-hour light/dark cycle to perform experiments during the dark, active phase. All experiments were approved by the local veterinary authorities in Zurich and conformed to the guidelines of the Swiss Animal Protection Law, Veterinary Office, Canton of Zurich (Act of Animal Protection 16 December 2005 and Animal Protection Ordinance 23 April 2008), animal welfare assurance numbers ZH165/19 and ZH224/15.

Humans

Patient data analysis was performed according to the ethical guidelines of the Canton of Zurich with approval from the local ethics committee ("PREDICT"; KEK-ZH-Nr. 2014-0304). From the Swiss Stroke Registry, we screened patients treated with acute ischemic stroke at the Department of Neurology, University Hospital Zurich from 01-04 2021 (n=202). Treatment decisions including thrombectomy were made by treating physicians according to current clinical guidelines. Stroke imaging including CT angiography (CTA), DSA and CT perfusion (CTP) was performed according to routine clinical protocols. We selected only those patients with distal MCA-M1 or M2 occlusion (one open MCA branch had to be identified for reference), who were sent to thrombectomy and had a successful recanalization result, corresponding to mTICI (modified treatment in cerebral infarction) grade 2b/3 (n= 26).[29] We excluded patients who objected to the use of their data for research purposes, or patients without any clinical follow-up information. Five patients were excluded because of insufficient quality of DSA data for semi-quantitative analysis, so that 21 patients were included.

Clinical information about sex, and age, and information about stroke severity according to the National Institute of Health Stroke Scale (NIHSS)[64] on admission as well as follow-up NIHSS and disability according to the modified Rankin Scale (mRS)[65] at 3 months post stroke were derived from the registry. Information about hemorrhagic transformation within the ischemic area was taken from clinical neuroradiology reports of brain MRI acquired one day after the intervention. Classification of LMC status as poor, intermediate, or good was done according to EXTEND-IA criteria.[66]

We found no association of sex with collateral status, early venous filling or haemorrhagic transformation of infarcts in the patient data.

METHOD DETAILS

Anaesthesia

For head-post and cranial window implantation, mice were anesthetized intraperitoneally with a mixture of fentanyl (0.05 mg/kg bodyweight; Sintenyl, Sintetica), midazolam (5 mg/kg bodyweight; Dormicum, Roche), and medetomidine (0.5 mg/kg bodyweight; Domitor, Orion Pharma). Throughout anaesthesia, a facemask provided oxygen at a rate of 500 ml/min. For stroke surgery and two-photon imaging anaesthesia was induced with isoflurane 4%, maintained at 1.2% with continuous supply of an oxygen/air mixture (30%/70%). For LSCI and ultrafast ultrasound recordings, anaesthesia was changed to a mixture of fentanyl (0.05 mg/kg bodyweight; Sintenyl, Sintetica), midazolam (5 mg/kg bodyweight; Dormicum, Roche), and medetomidine (0.5 mg/kg bodyweight; Domitor, Orion Pharma) before stroke induction. The core temperature of the animals were kept constant at 37°C using a homeothermic blanket heating system during all surgical and experimental procedures (Harvard Apparatus). The animal's head was fixed in a stereotaxic apparatus, and the eyes were kept moist with a vitamin A eye cream (Bausch & Lomb).

Head-Post Implantation

A bonding agent (Gluma Comfort Bond; Heraeus Kulzer) was applied to the cleaned skull and polymerized with a handheld blue light source (600 mW/cm^2; Demetron LC). A custom-made aluminum head post was connected to the bonding agent with dental cement (EvoFlow; Ivoclar Vivadent AG) for stable and reproducible fixation in the microscope setup. The skin lesion was treated with an antibiotic cream (Fucidin®, LEO Pharma GmbH)) and closed with acrylic glue (Histoacryl, B. Braun). After surgery, animals were kept warm and received analgesics (buprenorphine 0.1 mg/kg bodyweight; Sintetica).

Cranial window surgery

A 4 x 4 mm craniotomy was performed above the somatosensory cortex (centered above the left somatosensory cortex) with a dental drill (Bien-Air). A square coverslip (3 x 3 mm, UQG Optics) was placed on the exposed dura mater and fixed to the skull with dental cement.[67]

Thrombin stroke model

We induced a focal cerebral ischemia using the thrombin-model of stroke. The procedure steps for the cerebral ischemia induction were performed as described previously.[23,24,68] In brief, mice heads were fixed in a stereotactic frame, the skin between the left eye and ear was incised and the left temporal muscle retracted. After craniotomy above the middle cerebral artery (MCA) M2 segment, the dura was removed, and a glass pipette (calibrated at 15 mm/μl; Assistant ref. 555/5; Hoechst, Sondheim-Rhoen, Germany) was

introduced into the lumen of the MCA. Through the pipette, 1μl of purified human alpha-thrombin (1UI; HCT-0020, Haematologic Technologies Inc., USA) was injected to induce the formation of a clot in situ. Ten minutes after thrombin injection, the pipette was removed. Ischemia induction was considered successful when CBF rapidly dropped to at least 50 % of baseline level in the MCA territory[23,69] and remained below 50% for at least 30 minutes. Animals without stable ischemia induction were excluded from further experiments.

Rt-PA administration
Thirty minutes after ischemia induction, thrombolysis was initiated via tail vein injection of rt-PA (10 mg/kg, Actilyse, Boehringer Ingelheim). According to previous data,[23,70] ten percent were given as a bolus and ninety percent were perfused at a body weight dependent perfusion rate between 6 and 9.3μl/min. Control groups received the vehicle (0.9% saline) instead of rt-PA.

Laser Speckle Cortical Imaging (LSCI)
Cortical relative cerebral blood flow (CBF) changes were monitored before and during ischemia, and throughout the recanalization phase for 110 min using a laser speckle contrast imaging monitor (FLPI, Moor Instruments, UK). The acquisition was performed with a frame rate of 0.25 Hz. Afterwards the LSCI images were exported and generated with arbitrary units in a 256-colour palette by the MOOR-FLPI software.

Two-photon imaging
After cranial window implantation, mice could recover for 1-2 weeks prior to two-photon imaging. Imaging was performed using a custom-built two-photon laser scanning microscope (2PLSM)[71] with a tuneable pulsed laser (Chameleon Discovery TPC, Coherent Inc.) equipped with a 20x (W-Plan-Apochromat 20x/1.0 NA, Zeiss) water immersion objective. During measurements, the animals were head-fixed and kept under anaesthesia as described above. Vasculature was labelled with intravenous injection of FITC–dextran (2-MDa, Sigma-Aldrich; FD2000S) or Texas red Dextran (70 MDa, Life Technologies catalogue number D-1864), ten minutes before imaging. To visualize arterioles specifically, Hydrazide (Alexa Fluor™ 633 Hydrazide Life Technologies catalogue number A30634) was injected intravenously. Emission was detected with GaAsP photomultiplier modules (Hamamatsu Photonics) equipped with 475/64, 520/50 nm and 607/70 band pass filters and separated by506, 560 and 652 nm dichroic mirrors (BrightLine; Semrock). The microscope was controlled by a customized version of ScanImage (r3.8.1; Janelia Research Campus[62]). Baseline measurements were performed 90 min before induction of ischemia. Different branches from the MCA were identified based on the vascular anatomy. For acquisition of red blood cell (RBC) velocity and vessel diameters, line scans were performed in arterioles at 11.84 Hz, 0.55 μm/pixel and for 12.7 s. Three regions of interest (ROIs) were identified on the terminal distal branches of arterioles from the MCA. Three other ROIs were placed on collaterals, identified (1) as the arterio-arterial anastomosis connecting MCA to ACA and (2) by their typical tortuosity and low flow. The same vessels were evaluated before stroke, after stroke and throughout the experiment.

Line scans were processed with a custom-designed image processing toolbox for MATLAB (Cellular and Hemodynamic Image Processing Suite; R2014b; [https://doi.org/10.1007/s12021-017-9344-y]; MathWorks). Vessel diameters were determined at full width half maximum (FWHM) from a Gaussian fitted intensity profile drawn perpendicular to the vessel axis. RBC velocity flow was calculated with the Radon algorithm.

Ultrafast ultrasound imaging
Ultrafast ultrasound imaging (uUS) was performed on a prototype research ultrafast scanner with Neuroscan live acquisition software (ART Inserm U1273, Paris, France & Iconeus, Paris, France) using a 15 MHz ultrasound probe (0.11 mm pitch) which enables a 110 μm x 100 μm in plane resolution with a depth of 10 mm. The probe was mounted on 4 motors (3 translation + 1 rotation) for automatic positioning and scans. During measurements, the animals were head-fixed and kept under anaesthesia as described above.

4D Ultrasensitive Doppler
For each ultrafast Doppler image, 200 compounded frames (11 angles between -10°: 10°) were acquired at 500 Hz. Singular Value Decomposition clutter filters were used and the 60 first singular values were removed to separate blood signal from tissues. The energy in each pixel was calculated to form a Power Doppler image. The motor was then moved to cover 24 coronal slices imaged every 0.3 mm to reconstruct a 10 mm x 12.8 mm x 8 mm volume between β+2mm and β-6mm with a temporal resolution of 40 seconds. We performed a 10 minute recording for the baseline and two sets of recordings of 60 minutes each after stroke induction.

Automatic probe positioning
To enhance the reproducibility from one acquisition to another, the probe (before starting each 4D acquisition) was automatically positioned with the Brain Positioning System software[72] (Iconeus, Paris, France) over a coronal slice at Bregma minus 2.3 mm and aligned automatically to the Allen brain atlas.

Data processing

Within each acquisition (baseline, post-stroke1, post-stroke2), the volumes were realigned on the temporal average volume. Then, for each set of three acquisitions, a merged acquisition was created after registration of post-stroke1 and post-stroke2 acquisitions on the baseline and concatenation of baseline and the resulting registered post-stroke1 and post-stroke2 acquisitions.

Vascular Territories (VT) segmentation and CBV time-profile extraction

VT segmentation was performed manually on a baseline angiography reference.[72] Then, all the merged acquisitions were registered on this vascular reference. Hence, the same VT segmentation was used for all animals. Mean CBV time-profiles inside each Region of Interest (ROI) were extracted and normalized by the temporal average of the baseline acquisition to obtain relative-CBV (rCBV) curves.

Ultrasound Localization Microscopy

For each ultrasound localization microscopy (ULM) image, 100 μL of Sonovue® microbubbles (SonoVue, Bracco, Italy) were injected through a tail vein catheter. Every second 180 blocks of 800 compounded frames (3 angles at -5° 0° 5°) at 1000 Hz were acquired and reconstructed by a dedicated software (ART Inserm U1273, Paris, France & Iconeus, Paris, France). Briefly, a Singular Value Decomposition filter (removal of the 10 first singular values) was used to separate microbubble echoes from tissues and microbubble centroid positions were localized.[37] Microbubbles were tracked through consecutive frames, a tracking algorithm based on the Hungarian method for assignment. Tracks were interpolated and a density image was reconstructed by counting the number of tracks in each pixel of the grid. ULM was performed for 180 seconds before as well as one hour and two hours after stroke induction.

CO$_2$ challenge

To evoke hypercapnic hyperemia, mice were subjected to inhalation of 7.5% CO_2 (PanGas) for five minutes while anaesthetized with triple anaesthesia. At the same time, to assess cerebrovascular reactivity, blood flow was monitored using LSCI. The CO_2 challenge was administered once before induction of stroke and 60 minutes post-stroke. The maximum dilation of an artery was measured by evaluating an ROI on the most distal MCA segment (MCA-M5 supplied territory).

Tissue clearing

Mouse brains were stained for arteries and cleared using a modified version of the iDISCO protocol.[21] Mice were anesthetized, perfused, and the brains post-fixed in 4% PFA in PBS for 4.5 hours at 4°C, shaking at 40 rpm. Mouse brains were washed in PBS for 3 days at RT and 40 rpm, with daily solution exchange. Samples were dehydrated in serial incubations of 20%, 40%, 60%, 80% methanol (MeOH) in ddH$_2$O, followed by 2 times 100% MeOH, each for 1 hour at RT and 40 rpm. Pre-clearing was performed in 33% MeOH in dichloromethane (DCM) overnight (o.n.) at RT and 40 rpm. After 2 times washing in 100% MeOH each for 1 hour at RT and then 4°C at 40 rpm, bleaching was performed in 5% hydrogen peroxide in MeOH for 20 hours at 4°C and 40 rpm. Samples were rehydrated in serial incubations of 80%, 60%, 40%, and 20% MeOH in in ddH$_2$O, followed by PBS, each for 1 hour at RT and 40 rpm. Permeabilization was performed by incubating the mouse brains 2 times in 0.2% TritonX-100 in PBS each for 1 hour at RT and 40 rpm, followed by incubation in 0.2% TritonX-100 + 10% dimethyl sulfoxide (DMSO) + 2.3% glycine + 0.1% sodium azide (NaN3) in PBS for 5 days at 37°C and 65 rpm. Blocking was performed in 0.2% Tween-20 + 0.1% heparin (10 mg/ml) + 5% DMSO + 6% donkey serum in PBS for 2 days at 37°C and 65 rpm. Samples were stained gradually with Cy3-conjugated monoclonal anti-α-smooth muscle actin antibody (Sigma Aldrich, C6198) 1:800 in 0.2% Tween-20 + 0.1% heparin + 5% DMSO + 0.1% NaN3 in PBS (staining buffer) in a total volume of 1.5 ml per sample every week for 4 weeks at 37°C and 65 rpm. Washing steps were performed in staining buffer 5 times each for 1 hour, and then for 2 days at RT and 40 rpm. Clearing was started by dehydrating the samples in serial MeOH incubations as described above. Delipidation was performed in 33% MeOH in DCM o.n. at RT and 40 rpm, followed by 2 times 100% DCM each for 30 minutes at RT and 40 rpm. Refractive index (RI) matching was achieved in dibenzyl ether (DBE, RI = 1.56) for 4 hours at RT.

Whole-brain imaging

Three-D stacks of cleared brains were acquired using a custom-made selective plane illumination microscope (meso-SPIM, version V5)[73] (http://www.mesospim.org). One x zooms with a field of view of 1.3 cm and isotropic resolution of 6 μm/voxel. Imaging data were post-processed using Fiji (Image J, 1.8.0_172 64 bit) and Imaris (Oxford Instruments, 9.8.0).

Quantification of lesion volume and hemorrhages

At day 7 post stroke, mice were euthanized by receiving an overdose i.p. injection of pentobarbital (200 mg/kg) followed by decapitation. Brains were extracted and cut into 1 mm thick coronal slices from 6.5 to 0.5 mm anterior to the inter-aural line and placed in 2% 2,3,5-triphenyltetrazolium chloride (TTC, cat. #T8877, Sigma-Aldrich, St. Louis, MO) for 10 min at 37 °C. Infarct areas were determined by a blinded investigator using an image analysis system (Image J version 1.41). To correct for brain swelling, each infarct area was multiplied by the ratio of the surface of the intact (contralateral) hemisphere to the infarcted (ipsilateral) hemisphere at the same level. Total volume of damaged tissue, expressed as cubic millimetres, was calculated by linear integration of the corrected lesion

areas.[74] The presence of hemorrhage was recorded from TTC- stained brain slices at the time of premature death or sacrifice at day 7. Microscopic, macroscopic and total hemorrhagic scores were visually quantified on each level, from TTC- stained brain slices, as previously described.[75]

Behavioral assessment

Before stroke as well as on day 1, 3 and 7 post ischemia, neurological deficits were assessed using the adhesive tape removal test and a composite observational neurological score. In the adhesive tape removal test an investigator blinded to treatment applied two rectangular tape strips (0.3 × 0.4 cm) to both forepaws. In order to assess sensorimotor deficits, time was recorded until the animals first had contact (sensory function/neglect) and removed (motor function) both stripes.[76] Before stroke, mice were trained to remove both tapes within 10 seconds. In addition to the sticky tape test, the neurological score was obtained using a composite grading score as described before.[23] A lower score indicates larger neurological deficits, while a score of 13 points indicates no neurological deficit.

In-silico model

A full description of the in silico model is available in Epp et al.[12] Here, we provide a brief overview of the steps necessary to conduct in silico blood flow simulations with varying leptomeningeal collateral (LMC) densities. The *in silico* approach consists of three main steps: 1) microvascular network generation and modification, 2) in silico blood flow simulations, and 3) analyses of simulation results. Each of these steps is described in more detail below.

The four microvascular networks used for the *in silico* study (Figure 3A-B) were derived from in vivo surface artery (SA) networks of two C57BL/6 and two Balb-C mice. The networks are in the whisker and hindlimb area (MCA-M4/M5 territory) and span an approximate size of 3.5 x 3.5 mm^2. After manually tracing the topology, the networks were converted into graph format, and the density of descending arteriole (DA) root points was increased artificially to match values from in vivo quantifications in the respective mouse strains. To represent the complete cortical microvasculature DA and ascending venule (AV) trees were added to the SA network. DA and AV trees were then connected by an artificial capillary bed (Figure 3A).[77] As our focus is on the impact of LMCs we artificially added 4/7 LMCs to the SA networks of the two Balb-C mice, respectively (Figure 3B, bottom), to connect the areas fed by the MCA and ACA.

To further align our *in silico* framework to the *in vivo* flow field, we incorporated *in vivo* RBC velocity measurements (obtained from two-photon microscopy line scans) from the same networks via an inverse model. Additionally, literature data for DA and AV root vessels were added to the cost function of the inverse model. This allowed us to directly match the *in vivo* flow field at these measurement points and in parallel to reduce uncertainties in vessel diameters. The resulting four networks represent our baseline configurations for the case with 100% LMCs. To study the impact of collaterals half (50% LMCs) and all collaterals (0% LMC) have been removed (Figure 3B). In this context, it is important to note that for each of the four networks, the 100% LMC, the 50% LMC, and the 0% LMC case only differ in the number of LMCs but are completely equivalent otherwise. We refer to our related publication for the validation of the resulting networks and flow fields.[12]

The *in silico* blood flow model is well-established and can be derived from Poiseuille's law and mass conservation at bifurcations.[77,78] Here, we assumed a constant tube hematocrit of 0.3 and accounted for the Fahraeus-Lindqvist effect via an empirical *in vitro* formulation (Goyal et al.,[4]). For all simulations, we assigned a constant pressure drop between the Circle of Willis and the outlets of the ascending veins of 90 mmHg. Middle cerebral artery occlusion (MCAo) was modeled by a 90% constriction at the MCA-M2 bifurcation (Figure 3A). Additionally, the LMCs were dilated according to observations from *in vivo* experiments (average dilation factor of 1.7), and all SAs and DAs were dilated by 10%, mimicking a simplified autoregulatory response to MCAo.

Within this set-up blood flow simulations have been performed for the four distinct microvascular networks and the three levels of collateralization (0%, 50%, and 100% LMCs), resulting in twelve blood flow simulations. To comment on the impact of LMCs, the networks with no LMCs (0% LMCs) acted as our reference cases. Thus, the relative changes reported in Figures 3C and 3D are calculated by $(q^{sum}_{100\% \ LMC} - q^{sum}_{0\% \ LMC})/q^{sum}_{0\% \ LMC}$ and equivalently for 50% LMC. As the capillary bed is the primary location for oxygen and nutrient exchange, our analyses focused on the blood flow that reaches the capillaries. The flow sum of DA root points is a direct measure of the blood flow entering the capillary bed (Figures 3C and 3D). As MCAo heavily alters the pressure field, occasionally, we observed a flow reversal in DA root points (at maximum 9% of all DA roots per network). This phenomenon was most frequent for 0% LMCs and close to the watershed line. To comment on the amount of blood flow reaching the capillary bed, DA root points with flow reversal are not considered for the computation of the integral DA flow (i.e., the sum of all blood flow through DA roots). Additionally, the median relative change of capillary flow rate provides insights into perfusion changes at the capillary level (Figure 3E). The relative change of capillary flow in capillary *ij* is computed by $(q^{ij}_{100\% \ LMC} - q^{ij}_{0\% \ LMC})/q^{ij}_{0\% \ LMC}$. Further analyses with comparisons against baseline (i.e., without MCAo), in different vessel types, or without LMC- and SA/DA-dilations are available in our related publication.[12]

DSA data analysis

We collected biplane angiography runs obtained during the thrombectomy procedure with the in house angio-suite (Axiom-ArtisQ and Axiom-Artis Zee, biplane, Siemens, Germany) from the included patients. The standard protocol for image acquisition was to divide fluoroscopic acquisition into 3 phases; 10 images with a frame rate of 500ms, 5 images with 1s frame rate, and the remaining

Neuron
Article

CellPress
OPEN ACCESS

images with a frame rate of 2s for dose reduction. From each patient, only the image series from the final control runs where utilized. The corresponding DICOM images where anonymized and transferred to Fiji (Image J, 1.8.0_172 64 bit) for semiquantative analysis. Rather than specifying "arterial" or "parenchymal" early venous filling,[57] we used the open source "time lapse color coder" module from ImageJ to allow visual representation of contrast filling delays in angiographic images. To do this, the first frame of arterial filling till the last frame of the DSA images were manually selected and each frame was coloured according to a pseudocolor LUT (look up table) to display even small time delays with maximum visibility. As all our cases had at least one non-occluded MCA branch, we took this territory as an internal reference for venous delay in this patient. Dichotomous visual assessment of venous filling delays into "early venous filling" (i.e., clear difference of one or more venous drainage territories of the affected hemisphere) and "no early venous filling" was done on maximum intensity projections of the color-coded time series based on apparent temporal encoded colour differences in venous delay. Two interventional neuroradiologists, unaware of clinical or imaging outcome, performed the readings and assessments independently.

QUANTIFICATION AND STATISTICAL ANALYSIS

Data in all groups was tested for normality using D'Agostino-Pearson omnibus normality test. Parametric statistics were used only if the data in all groups in the comparison were normally distributed. Statistical analysis was performed using the GraphPad Prism (version 8.0; GraphPad Software La Jolla, CA, USA). All statistical tests and group size (n) are indicated in the figures. To account for multiple observations within the imaged mouse, results from each group were compared using univariate nested model t-tests before proceeding with the discriminant analysis. Results were expressed either as mean ± s.e.m. (standard error of mean), or median (interquartile range) in box plots. Comparisons between patient groups were done using IBM SPSS Statistics (Version 27, 28). Significance ($P < 0.05$) between two groups was calculated using unpaired Student's t-test or paired t-test for normally distributed data, or with the Mann–Whitney test for data with non-normal distribution. Frequencies were compared using the Chi Square test.

We found no association of sex with collateral status, early venous filling or haemorrhagic transformation of infarcts in the patient data.